Development of mechanical strengthening system for bridge connections using prestressed CFRP rods

Hossein Heydarinouri [1]; Masoud Motavalli [2]; Alain Nussbaumer, M.ASCE [3]; Elyas Ghafoori, M.ASCE [4]

[1] Ph.D. candidate, Empa, Swiss Federal Laboratories for Materials Science and Technology and Swiss Federal Institute of Technology Lausanne (EPFL). Ueberlandstrasse 129, 8600 Duebendorf, Switzerland, Lausanne, Switzerland. E-mail: hossein.heydarinouri@empa.ch

[2] Professor, Head of the Structural Engineering Research Laboratory, Empa, Swiss Federal Laboratories for Materials Science and Technology, Ueberlandstrasse 129, 8600 Duebendorf, Switzerland. E-mail: masoud.motavalli@empa.ch

[3] Professor, Resilient Steel Structures Laboratory, Swiss Federal Institute of Technology Lausanne (EPFL), Lausanne, Switzerland. ORCID: http://orcid.org/0000-0002-8994-4926. E-mail: alain.nussbaumer@epfl.ch

[*4] Group leader, Scientist, Empa, Swiss Federal Laboratories for Materials Science and Technology, Ueberlandstrasse 129, 8600 Duebendorf, Switzerland (Corresponding Author). ORCID: http://orcid.org/0000-0002-4924-0668. E-mail: elyas.ghafoori@empa.ch

Abstract

Stringer-to-floor beam web-to-web double-angle connections are among the most fatigue-prone elements in old riveted bridges. These connections are often designed to carry only shear loads. However, in these elements, fatigue damage occurs because of the out-of-plane deformation of the connections, which is ignored in the original design. In this study, a new retrofitting system is developed to reduce the out-of-plane deformation of the connections using prestressed carbon

This document is the accepted manuscript version of the following article:
Heydarinouri, H., Motavalli, M., Nussbaumer, A., & Ghafoori, E. (2021). Development of mechanical strengthening system for bridge connections using prestressed CFRP rods. Journal of Structural Engineering, 147(3), 4020351 (19 pp.).
https://doi.org/10.1061/(ASCE)ST.1943-541X.0002923

fiber reinforced polymer (CFRP) rods. The proposed system consists of a mechanical wedge-barrel anchor to hold the prestressed CFRP rod and a clamping system to attach to the parent structure and to transmit forces via friction. A series of finite element (FE) simulations was conducted to optimize the size and performance of the retrofit system. Laboratory static pull-off tests were conducted and different failure modes were studied and discussed. A novel test set-up (with four supports) was designed for testing the steel connections. The effect of the geometrical imperfections during the installation of the connection was carefully investigated using the FE models and was verified through laboratory the tests. Laboratory fatigue tests were conducted on steel connections with the same dimensions as those in a railway bridge. The designed retrofit system was found to be capable of reducing the stresses at the angle connections by more than 40%. The results of the fatigue tests demonstrated that the designed system could survive more than 11 million load cycles without any fatigue damage or any indication of a loss in the CFRP prestressing level.

Keywords: Bridge connections, Carbon fiber-reinforced polymer (CFRP), Finite element (FE), Post-tensioned CFRP tendons, Strengthening, Wedge-barrel anchor.

Introduction

Fatigue is a major problem in aging steel bridges in Europe. This problem is further exacerbated in old steel bridges, which are approaching the end of their originally designed fatigue lives (Ghafoori 2019). Most of the old metallic bridges in Europe are riveted bridges. In these bridges, the stringer-to-floor-beam double angle web-to-web connections are one of the most common fatigue prone details (Haghani et al. 2012).

Out-of-plane deformation of the angles is the primary reason for the fatigue problem in this type of connections (Fisher et al. 1987, Fisher et al. 1990, Al-Emrani and Kliger 2009). The out-of-plane deformation results from the application of the loads on the stringers, leading to secondary deformation-induced tensile stresses in the connections. In the past, this effect was

not considered in the design; therefore, the engineers would design the connections to carry only shear loads. Owing to the out-of-plane deformation, the fatigue failure can occur either in the angle (near the fillet) or in the rivets (popping out of the rivet head) (Al-Emrani 2002). The out-of-plane deformation due to the superimposed loads on the stringers, as well as the potential failure locations in the connections, are schematically illustrated in Fig. 1-a.

The replacement of the bridges to address the fatigue related failures of the bridges is rarely a preferred solution for the owners of the bridges. Therefore, they always look for effective and sustainable strengthening solutions. Until now, many different strengthening techniques have been proposed for the prolongation of the fatigue life of riveted structures, such as replacement of rivets with high-strength bolts (Reemsnyder 1975; Baker and Kulak 1985; Al-Emrani 2002), using stop holes and welding additional elements (Kuehn et al. 2008), and softening connections by removing some rivets (Bowman 2012). The drawback of these strengthening solutions is that they are not capable of permanently addressing the problem — when these solutions were tried, the fatigue cracks have either reinitiated after a certain number of cycles or have initiated from another location (see (Roeder et al. 2005)).

New materials, such as carbon fiber reinforced polymers (CFRP) have been used for strengthening metallic structures as non-prestressed bonded retrofitting systems (Mertz and Gillespie 1996; Dawood et al. 2007; Schnerch et al. 2007; Haghani et al. 2009; Haghani 2014) owing to their superior fatigue and corrosion resistance and light weight compared to steel (Zhao 2013). However, in several cases, bonded systems cannot be applied on the surface of riveted members.

Recently, prestressed unbonded reinforcement (PUR) systems have been developed for strengthening bridge structures (Ghafoori et al. 2012, Ghafoori and Motavalli 2015a). Different configurations of the PUR systems, i.e., trapezoidal PUR (TPUR), flat PUR (FPUR), contact PUR (CPUR), and triangle PUR (TrPUR) have been designed, and their performances have been examined numerically and analytically (Kianmofrad et al. 2017). Such systems consist of

mechanical clamps holding prestressed CFRP plates and working purely through friction. The PUR systems can be used for strengthening steel beams against flexural (Hosseini et al. 2018c), buckling (Ghafoori and Motavalli 2015b), and fatigue (Ghafoori et al. 2015b) loading. These systems were successfully used for strengthening old steel bridge girders in Switzerland (Ghafoori et al. 2015a) and Australia (Ghafoori et al. 2018; Hosseini et al. 2019a). More recently, a series of PUR systems has been developed for strengthening steel plates (Hosseini et al. 2018b; Hosseini et al. 2019b). The PUR concept has also been used with shape memory alloy (SMA) plates (instead of CFRP plates). SMAs are a new class of structural materials that can be prestressed through an activation process that includes heating and cooling (Hosseini et al. 2019c). The SMA-based PUR systems have been using for strengthening steel plates (Izadi et al. 2018a; Izadi et al. 2018b), girders (Fritsch et al. 2019; Izadi et al. 2019a) and connections (Izadi et al. 2019b).

Knowledge gap and objectives of the study

Nearly all the aforementioned retrofitting solutions are applicable only to steel girders and plates, and not to the connections. For stringer-to-floor beam double angle connections, finding an effective strengthening solution is a considerable challenge owing to a lack of space, as well as additional complexity of the geometry in these details. Hence, sufficient research has not been conducted on the strengthening of bridge connections (unlike in the case of bridge girders). In fact, in such design elements, the existence of floor-beams and other elements, such as sleepers renders the application of CFRP plates almost impossible. For similar reasons, the system proposed in (Izadi et al. 2019b), in which prestressed SMA plates were used for strengthening stringer-to-floor-beam double angle connections, may not be applicable in real structures, although its performance was proven through laboratory tests.

Considering the aforementioned issues, this study, for the first time, proposes the application of prestressed CFRP rods for strengthening bridge connections. Thus far, different mechanical anchorages have been developed for post-tensioned CFRP rods (Sayed-Ahmed and

Shrive 1998; Campbell et al. 2000; Al-Mayah et al. 2005; Al-Mayah et al. 2006a, 2007; Schmidt et al. 2010; Schmidt et al. 2011; Schmidt et al. 2012). In these studies, the proposed mechanical anchorages consisted of a barrel with a conical hole inside, and split or integrated wedges holding the CFRP rod. Such anchors have been already used for externally prestressed concrete beams (Bennitz et al. 2012). These mechanical anchors hold the CFRP rod through friction, without requiring any adhesive, thus increasing their versatility for on-site applications compared to bonded systems, an example of which was proposed in (Meier 1995).

In this study, a novel mechanical strengthening system using prestressed CFRP rod is proposed. The proposed strengthening system in this study is a combination of the clamping system proposed in (Ghafoori 2015; Hosseini et al. 2018a) and the idea of using a CFRP rod as a prestressing element. In previous PUR systems, two symmetric prestressed CFRP elements are required. However, the proposed system operates with unsymmetrical prestressed CFRP elements; this feature increases its versatility and adaptability for applications to various types of structures.

A conceptual representation of the proposed strengthening system is illustrated in Fig. 1-b. Here, the out-of-plane deformation of the angles is reduced, i.e., the prestressed CFRP rods apply a compressive load P on both sides of the stringers. In addition, the prestressing force applies a sagging moment, M_p, opposing the out-of-plane deformation of the angles, which results in a reduction in the secondary stresses in the angles.

Furthermore, the proposed system uses a novel wedge-barrel anchor component, which was developed at the Structural Engineering Research Laboratory at Empa, Switzerland. This study mainly focuses on the behavior of the entire clamping system; however, a brief description of the developed wedge-barrel anchor and the main experimental results are also presented here.

In addition, one of the main challenges in the existing wedge-barrel anchors is the requirement of a high presetting force; in other words, before pulling the CFRP rod, to increase the

127 contact pressure around the CFRP rod, the wedges have to be pushed (preset) into the barrel.
128 Otherwise, when pulled, the CFRP rod would slip inside the wedges. In this study, a new pre-
129 setting system for on-site application of high forces is developed, which obviates the need for
130 using hydraulic jacks.

131 ***Outline of the study***

132 This paper outlines the introduction of a retrofitting system concept, including the installa-
133 tion of a clamping system, as well as presetting and prestressing procedures. Subsequently,
134 results from static pull-off tests are presented and discussed. Thereafter, a finite element (FE)
135 model, developed for designing the clamping system, is presented. The investigation of the
136 fatigue performance of the proposed strengthening system is also discussed. The effectiveness
137 of the proposed system in reducing the secondary deformation-induced stresses in the connec-
138 tions is investigated both numerically and experimentally. Finally, the application of the pro-
139 posed strengthening system on an old riveted railway bridge in Switzerland is briefly described.

140 **Introduction to the strengthening system**

141 ***Description of the clamping system***

142 The configuration of the proposed strengthening system is shown in Fig. 2-a. It consists of
143 two main components, the mechanical wedge-barrel anchor and the clamping system, as shown
144 in the figure. The wedge-barrel anchor holds the prestressed CFRP rod, and the clamping sys-
145 tem grabs the top flange of the stringer and transmits the CFRP prestressing force to the stringer
146 through friction.

147 The two aforementioned components consist of different parts, as shown in Fig. 2-b. The
148 wedge-barrel anchor consists of a barrel with a conical hole inside and three separate aluminum
149 wedges, which are in direct contact with the CFRP rod. The clamping system is assembled from
150 different plates, which are bolted to each other. For assembling the clamping system, first, the
151 bottom plate, the vertical plate, and the two stiffeners are bolted to each other. The bolts are

M16, 12.9 and M12, 12.9 , with clamping forces of 135 and 72 kN, respectively. The spacer is also bolted to the bottom plate using two M4 bolts, which fix the spacer in the position. Next, the top plate is placed on top of the beam top flange, and then the top and bottom plates are connected to each other using four M20, 12.9 bolts. A total compressive force of 484 kN is applied to the top flange by these bolts to prevent the clamping system from slipping through friction. Thus, through the wedge-barrel anchor, the prestressing force of the CFRP rod is transmitted to the clamping system by a threaded hollow shaft in the vertical plate. All the plates in the clamping system are made of M200 high-strength steel with a nominal yield strength of approximately 1000 MPa. The details of the dimensions of the clamping system components are given in Fig. A1 in the appendix.

As mentioned before, in the PUR system proposed by (Ghafoori 2015, Hosseini et al. 2018a), prestressed CFRP plates were used for strengthening the girders. However, the presence of floor-beams, together with sleepers resting on the stringers rendered it impossible to use CFRP plates. Instead, in this study, a prestressed CFRP rod is used. Here, the CFRP rod passes through a rivet/bolt hole, as shown in Fig. 2-a, and requires removal of the rivets/bolt prior to strengthening. It is noted that the rivets/bolts are removed from the second row of the rivets/bolts (see Fig. 2-a) and their absence does not affect the out-of-plane deformation of the connections (Munse and Petersen 1959; Kulak et al. 2001). In addition, hollow high-strength bolts are placed and fastened, as a replacement for the removed rivets/bolts. The CFRP rods then pass through the hollow bolts. The main aim of using hollow bolts is to prevent corrosion inside the opening hole caused by the removal of the rivet/bolt.

Installation procedure

The strengthening system is installed in two stages: presetting and prestressing. These two stages are described in the following sections.

Presetting procedure

In the proposed strengthening system, presetting is performed as shown in Fig. 3-a to c. The parts required for presetting are shown in Fig. 3-a. The presetting steps are outlined as follows: Once the clamping system is fixed, the CFRP rod passes the threaded hollow shaft, and the barrel and the wedges are placed around it. Then, the presetting shaft, which has a specific length, is placed around the wedges on the barrel. At the free end of the barrel, there is a threaded region, which allows the placement of the presetting ring around the barrel, as shown in Fig. 3-a and b. Then, the presetting plate is placed on the wedges, and six M8 presetting bolts pass through the presetting plate and the threaded holes of the presetting ring. Before the presetting bolts are fastened, a gap exists between the presetting plate and the presetting shaft, as shown in Fig. 3-b. By fastening the bolts, the presetting plate pushes the wedges into the barrel. The bolts are fastened until the prestressing plate touches the presetting shaft; at this point, the presetting is completed. With the six M8, 8.8 bolts, it is possible to apply a total force of approximately 110 kN. The length of the presetting shaft was determined based on the tests to ensure that when the shaft touches the presetting plate, adequate presetting force is applied to the wedges.

It is important to note that in the proposed system, the CFRP rod has to, first, pass through a small hole (rivet or bolt hole) in the floor beam, and then, it should be clamped on the other side as shown in Fig. 2-a. Thus, it is not possible to carry out the presetting procedure for both active and dead anchors in advance using hydraulic jacks; i.e., only one anchor can be prepared beforehand and the other one has to be preset on-site.

In addition, to prevent the rotation of the wedge-barrel anchor during the fastening of the presetting bolts, two presetting walls are connected to the stiffeners. Next, the two stiffeners are connected to the prestressing ring using two M8 bolts, as illustrated in Fig. 3-b and c. Once the presetting is completed, the presetting walls are removed; however, the other parts used for presetting are kept in place to be used later for prestressing the rod.

Prestressing procedure

After the wedges are preset, the CFRP rod is ready to be pulled. To apply the prestressing force, a temporary housing is used, as shown in Fig. 3-d. The housing consists of three plates connected to each other by M16, 12.9 bolts. Further details regarding the housing components are shown in Fig. A2 in the appendix. The housing is fixed on the clamping system using two M8 threaded rods. Next, a high-strength M13 threaded rod is inserted into the threaded hole embedded in the presetting plate. The tensile strength of this rod is 150 kN.

In the final step, a 120-kN hydraulic cylinder provides the pulling force (see Fig. 3-d) for the prestressing procedure. When the CFRP rod is pulled, the barrel moves away from the surface of the threaded shaft. Once the required prestressing force is reached, the threaded shaft is rotated until it touches the back of the barrel. At this stage, the system is fixed; the oil pressure in the hydraulic cylinder is released; and the housing and the plates required for presetting and prestressing are removed.

Dismantling procedure

To disassemble the system, the same procedure as shown in Fig. 3-d can be followed. In the first step, a pulling force slightly higher than the existing prestressing force in the CFRP is provided by the hydraulic cylinder. Thus, the barrel becomes separated from the threaded shaft; therefore, it is possible to take the shaft out (away from the barrel). Finally, the oil pressure in the hydraulic cylinder is released; consequently, the CFRP prestressing force is removed. To ensure practicality, before the application of the pulling load by the cylinder, the cylinder should have an adequate displacement capacity to release all the oil pressure.

Advantages of the proposed retrofit system

Most existing solutions for strengthening bridges have been designed for bridge girders rather than for connections. Strengthening of connections is often difficult owing to issues, such as the need for removal of the decks, lack of space, and geometric complexities. This study aims to present a system for retrofitting the connections using CFRP composites. There are two main

differences between the system proposed in this study and the previously developed PUR systems. The first difference is that in this study, an unsymmetrical clamp was used, which provides increased freedom and versatility to apply this system to different structures with edges. On the other hand, the previous PUR systems have utilized two CFRP plates, placed symmetrically in the clamping system. The second difference is that unlike the previous PUR systems, which all worked with CFRP plates as mentioned above (Kianmofrad et al. 2017), the PUR system developed in this study uses CFRP rods, as they can be easily passed through the connection by removing bolts/rivets.

One of the main advantages of the proposed strengthening concept for bridge connections in this study is that it works only by accessing the system from the lower part of the bridge (i.e., flooring system) without requiring the removal of the bridge deck. Therefore, the proposed strengthening system can be used for strengthening of the bridge connections with minimum interventions, i.e., it requires no bridge closure, no interruptions for the traffic on the bridge, and no holes to be drilled in the parent structure. Finally, the proposed system can also be considered, in some cases, for other types of connections, such as welded connections.

Static and fatigue tests on wedge-barrel anchors

One of the key components of the proposed strengthening system is the wedge-barrel anchor that holds the CFRP rod. A new, purely mechanical wedge-barrel anchor was developed in Empa, Switzerland for this purpose. To ensure that the anchor performs reliably under both static and fatigue loadings, a series of tests was conducted according to European Technical Approval Guidelines ETAG 013 (EOTA 2002); the FIP recommendation for post-tensioning systems (Recommendation 1993); and the draft guideline for the acceptance testing of FRP post-tensioning tendons (Rostásy 1998).

The test set-up used for the uniaxial tensile static and fatigue tests on the wedge-barrel anchors with a CFRP rod having an 8-mm diameter is shown in Fig. 4-a, with a nominal tensile

strength of 102.9 kN. A cover was used around the CFRP rod to limit the dispersion of the fibers after a rupture. The mechanical wedge-barrel anchor consists of a steel barrel in contact with three split aluminum wedges holding the CFRP rod. The components of the wedge-barrel anchor are shown in Fig. 4-b.

The experimental results indicate that the developed wedge-barrel satisfies all the requirements listed by the above-mentioned codes and recommendations. The results are summarized as follows:

The static tests indicate that the fracture of the CFRP rod was the failure mode and not the slippage of the CFRP rod inside the barrel. For each static test, the failure load of the post-tensioned system was higher than 95% of the nominal tensile strength of the CFRP rod. The average failure load was 119 kN (equivalent to approximately 2370 MPa for the CFRP rod with 8-mm diameter).

During the fatigue loading for 2 million cycles, no failure occurred either in the CFRP rod or in the anchor, and no slippage was observed between different components of the wedge-barrel. In addition, at the end of the fatigue test, a static test was carried out, which showed no reduction in the residual static strength of the anchor system, indicating that during the fatigue loading, no significant damage was accumulated in the anchors.

In addition, further verification of the anchor behavior with respect to slippage was carried out by increasing the loading frequency up to 23 Hz in the fatigue tests. All the tests confirmed that no slippage occurred in the anchorage system under fatigue loads. All subsequent tests described in the next sections confirmed this excellent behavior; i.e., the rods suffered neither slippage nor any significant damage in the wedge-barrel anchorage system.

Static pull-off tests

To experimentally investigate the static performance of the strengthening system, static pull-off tests were performed in the test set-up shown in Fig. 5. In these tests, the goal was to

obtain the failure load of the CFRP rod and the slippage load of the clamping system.

Test set-up and instrumentation

A clamping system was installed on either side of an IPB 400 beam. The geometrical dimensions (i.e., cross-section) of the beam used in the set-up were the same as those used in the Aabach Bridge, which is an old riveted railway bridge in Switzerland. The reason for this choice was that the retrofit system was designed for strengthening the connections of this bridge. The length of the beam was 1.5 m. The pulling force was applied using two 200-kN hydraulic cylinders, and the applied load was measured using a 150-kN load cell (HBM AG, Germany) with an accuracy of 0.2 kN. The detailed dimensions of the set-up are provided in Fig. A3 in the appendix.

The unidirectional CFRP rod used in the pull-off tests was manufactured by S&P Clever Reinforcement Company AG, Switzerland, with a diameter of 8 mm. The nominal tensile strength (the guaranteed value) of the CFRP rod, F_u, was 102.9 kN (equivalent to 2047 MPa), with a fiber volume fraction of 65% and an elastic modulus of 160 GPa in the fiber direction.

The instrumentation used in the static pull-off test is shown in Fig. 6-a. When the CFRP rod was being pulled, a line laser model 2660-50 (MICRO-EPSILON, Germany) with a resolution of 4 μm was used to measure the displacement of different components of the wedge-barrel anchor, i.e., the CFRP rod, two of the wedges, and the barrel. In addition, the displacements of the top plates of the clamping system were measured using two linear variable differential transformers (LVDTs).

It should be noted that in these tests, the CFRP rod was used on only one side of the beam, while a high-strength steel rod (with a tensile strength of 150 kN) was used on the other side (see Fig. 6-b). This would ensure that the beam would be symmetrically loaded, and, the failure

would occur solely in the CFRP rod/anchorage. Thus, it would be possible to focus on the behavior of the anchor on the side with the CFRP rod, and to perform the measurements only on this side.

Results of the static pull-off tests

Based on the loading protocol proposed by the draft guidelines for the acceptance testing of FRP post-tensioning tendons (Rostásy 1998), the cylinder load was increased stepwise, as shown in Fig. 7-a. The applied cylinder load in the pull-off tests P is shown in Fig. 7-b, in which the oil pressure in the cylinder was kept constant for 5 min at steps A, B and C, and more than 1 h at step D. This loading protocol was proposed to ensure that the displacements in the wedge-barrel anchor were stabilized after 0.5 h at step D.

The displacements of the wedge-barrel components were measured by the line laser during the load steps A to D, as illustrated in Fig. 8-a. As shown in the figure, for the duration of all the different steps, the displacements were quite stable indicating that there was no gradual slippage in the wedge-barrel anchors.

In addition, the relative displacement of the two wedges and the CFRP rod with respect to the barrel, called the draw-in, versus the applied load is plotted in Fig. 8-b. This figure shows that at the load levels slightly lower than 70 kN, the wedges and the CFRP started going into the barrel simultaneously. It shows that there was no relative displacement between the CFRP rod and the wedges. This is the ideal behavior for the wedge-barrel anchors because when the wedges and the rod are inserted into the barrel simultaneously, the contact pressure around the rod increases, leading to an increase in the frictional resistance.

At the end of step D, the cylinder load was reduced (see Fig. 7-b) to around 30 kN, and then, the line laser was removed to prevent the laser from being damaged at the failure load of the CFRP rod. Then, the CFRP was loaded up to failure. In total, four static pull-off tests were conducted. In one of the tests (Test no. 1), a strain gauge was applied on the CFRP rod. The

326 measurement showed a linear stress–strain behavior, with an elastic modulus of 160 GPa, which
327 was in good agreement with the value provided by the manufacturer.

328 The results of the four pull-off tests are summarized in Table 1, based on which it can be
329 concluded that failure occurred in the CFRP rod. No slippage could be observed in the clamping
330 system. The obtained failure load in all the tests was higher than the nominal failure load of the
331 rods, which was equal to 102.9 kN (equivalent to 2047 MPa). The average failure load of the
332 pull-off tests was equal to 110 kN (equivalent to 2188 MPa), which was only 9 kN lower than
333 the average value obtained in the uniaxial tensile tests on the rods.

334 It is worth mentioning that the force in the CFRP rod would tend to rotate the clamping
335 system. The rotation of the clamping system and the consequent rotation of the barrel would
336 apply bending stresses on the loading end of the wedge-barrel anchor, which could ultimately
337 lead to a premature rupture in the CFRP rod. However, the high average failure load obtained
338 in the pull-off tests shows that the clamping system was rigid enough to minimize the rotation.
339 Therefore, it can be concluded that the failure load of the CFRP rods was only marginally af-
340 fected. The displacement of the clamp, measured using the LVDTs, during the pulling of the
341 CFRP rod and a failed sample (sample no. 4) is shown in in Fig. 9.

342 To obtain the slippage load of the clamping system, high-strength steel rods, as shown in
343 Fig. 6-b, were used on both sides of the beam to ensure that slippage of the clamp would not
344 occur before the failure of the rods. The slippage load is defined as the load at which the dis-
345 placement of the entire clamping system in the load direction increases suddenly. The test re-
346 sult, as depicted in Fig. 10, shows that the slippage load of the clamping system was 128 kN, at
347 which slippage occurred in one of the clamps. The slippage load was higher than the ultimate
348 strength of the CFRP rods.

349 **Finite Element (FE) model**

350 ***Description of the model***

An FE model was developed for different parts of the clamping system, as illustrated in Fig. 11, using the ABAQUS FEM software. In the FE analysis, the clamping system components were modeled as 3D solid parts. Due to the symmetry, only half of the beam IPB400, with a length of 1.5 m, was considered. The parts were modeled with an isotropic elastic material having an elastic modulus of 200 GPa and a Poisson's ratio of 0.3.

The boundary conditions used in the model are depicted in Fig. 11. In the plane of symmetry, which lies in the middle of the beam web, the displacement, U_x, and the rotations, U_{ry} and U_{rz}, were assumed to be zero. In the horizontal and vertical supports, the movements of the surfaces shown in Fig. 11 in the *z*- and *y*- directions, respectively, were constrained.

In addition, to consider the effect of the M20 bolts, which connected the top and bottom plates to each other, the surface of each hole in the top plate was tied to its corresponding hole surface in the bottom plate. A tie constraint makes the active degrees of freedom (i.e., translational and rotational motion) of the tied surfaces equal so that there is no relative motion between them. Therefore, using the tie constraint, it was ensured that the top and bottom plates would move simultaneously in the event of a slippage.

The analysis was performed through different steps, as outlined below:

(1) Bolt load: in the first step after the initial step (in which the boundary conditions were applied), the resultant force exerted by each bolt was applied; Each M20 12.9 bolt applied a total force of 212 kN on the top plate. In the FE model, this force was applied as a shear traction of 840.4 MPa to the surface of the holes in the top plate. These bolts would apply the same load to the bottom plate through the bolt head and it was applied as a pressure load. The bolts M16 12.9 and M12 12.9 also applied 135 and 72 kN, respectively, through both shear traction or pressure load as shown in Fig. 11.

(2) CFRP load: In the proposed system, the tensile load of the CFRP was applied to the clamping system from the barrel to threaded hollow shaft. In the FE model, the CFRP

force was applied to the threaded shaft as a pressure load on an area where the barrel touched the shaft, as demonstrated in Fig. 11.

Different formulations and approaches have been conducted for modeling the contact behavior between different interfaces (Schmidt et al. 2011; (Al-Mayah et al. 2006b). In this study, similar to the approach conducted in (Schmidt et al. 2011), a surface-to-surface master/slave discretization was used for modelling the contact between different interfaces using finite sliding formulation, indicating that the separation and the arbitrary finite sliding and rotation of the surfaces were allowed. To have an identical sliding properties in all directions, isotropic directionality was selected (Dassault Systèmes 2014). The normal contact behavior was modeled as "Hard Contact," which would prevent the parts from penetrating each other. The tangential contact behavior was considered using the penalty friction formulation, which permits a small relative motion (i.e., a small fraction of the element size) of the surfaces before the surface traction reaches a critical shear stress (Dassault Systèmes 2014). The critical shear stress is obtained by multiplying the normal contact pressure by the surface friction coefficient. The small relative motion in the penalty friction formulation prevents from the convergence problems due to the discontinuity between the sticking and slipping states. Further in-depth information about different methodologies for modeling the contact for the interfaces as well as the required formulations are given in (Wriggers and Zavarise 2004). In this study, the friction coefficient between the top and bottom plate with the top flange of the beam was determined via verification with the experimental result, as described before.

The elements in the beam, and top, bottom, and vertical plates, in which the bending deformation was dominant, were discretized into quadratic reduced-integration elements, while the other parts were discretized into linear elements. It is noted that on one hand, the use of quadratic elements rather than linear elements increases the computational cost because for these elements, the strain and stress fields have to be computed for a larger number of integration points. On the other hand, the linear elements are not an appropriate choice in bending unless

the mesh is made extremely fine, resulting in an increased computational cost. Therefore, in the FE model, the quadratic reduced-integration elements were used for the parts with the dominant bending deformations.

The free mesh type was adopted for the top and bottom plates; for the threaded hollow shaft, beam, and spacer a structured mesh was used; and for the stiffeners a sweeping mesh was used. Different meshing techniques, i.e., sweeping, structured, and free meshes, were chosen based on the complexity of each part's geometry. To account for the mesh size effect, different mesh sizes were selected, as described before.

Correlation between the FE model and experimental results

To verify the FE model with the experiment, the obtained value of the slippage load in the FE model was compared with the experimental results. The slippage load depended on the friction coefficient of the surfaces between the top and bottom plates of the clamping system, and the top flange of the beam. After considering different friction coefficients for these surfaces, a value of 0.16 was found to lead to a slippage load of 125 kN for the clamping system, which is very close to the 128 kN obtained in the experiment, as shown in Fig. 12-a. In this figure, the displacement of the entire clamping system (a node on the top plate) in the loading direction, U_{Clamp}, is plotted against the applied load, P.

In addition, the parametric analysis on the friction coefficient showed that the slippage load and the stress distribution in the clamping system do not depend on the friction coefficient between the stiffeners, and between the vertical and bottom plates, as long as this coefficient was greater than 0.1. With a friction coefficient lower than 0.1, a slippage would occur between the vertical plate and the stiffeners before the slippage of the whole clamping system. However, as such a slippage was not observed in the experiment, the same value of 0.16 for the friction coefficient was considered throughout the model.

Two different types of meshes, a fine mesh and a course mesh, were considered to investigate the effect of mesh size, the details of which are summarized in Table 2. The mesh size in regions, where the bending deformation was dominant, and where slippage could occur was changed. Therefore, as given in the table, the mesh sizes for the top, bottom, and vertical plates, as well as the fine mesh region of the beam were different for the fine and coarse mesh cases. The mesh size for the other parts was the same for the two cases. As shown in Fig. 12-a, a change in the mesh size in the two different mesh size cases did not influence the obtained slippage load.

In addition, in Fig. 12-b, the displacement of the barrel in the z-direction, measured by the line laser, was compared with that obtained from the FE model. As shown in the figure, the change in the mesh size did not have a significant effect on the obtained displacement.

Furthermore, the FE model showed that the displacement of the threaded hollow shaft, U_{Shaft}, was not dependent on the value of the friction coefficient between the stiffeners and the vertical and bottom plates at the load levels of 70–80 kN (which can be inferred from Fig. 12-b), even for a friction coefficient less than 0.1. The reason for this behavior is that the bolts connecting these parts provided sufficient friction resistance, particularly at the aforementioned low load levels.

In the FE model, it was assumed that the displacement of the barrel was equal to the displacement of the hollow shaft. This assumption was valid because the axial displacement of the barrel could be ignored. The displacement of the barrel (or the threaded hollow shaft) was greater than that for the whole clamping system (shown in Fig. 12-a), which was because of the rotation of the clamping system, as well as the bending deformations due to the applied load.

Notably, as shown in Fig. 11, the von Mises stress in different parts of the clamping system was lower than the yield stress of the material, i.e., 1000 MPa, at the slippage load. However, under the service loads, the applied load to the clamping system was further lower; For example,

for the CFRP rod used in the experiments in this study, the maximum load in the acceptance tests (based on ETAG 013 (EOTA 2002) and (Recommendation 1993)) in the CFRP rod was 66.9 kN (equivalent to 1331 MPa).

Tensile stress in the top flange of the beam

One of the most important considerations for designing the clamping system is the bending stresses generated in the top flange of the beam due to the rotation of the clamping system. As shown in Fig. 13, when the CFRP load was applied to the clamping system, there were two regions in the beam top flange with high tensile bending stresses σ_b. As shown in Fig. 13, due to the application of a CFRP load of 125 kN, the tensile bending stresses in the bottom and top of the beam top flange were 293 and 297 MPa, respectively, which were smaller than the yield stress of the beam material (the beam was made of S235 steel with a yield strength of 380 MPa according to the coupon tests.). In addition, the FE model showed that the tensile bending stresses in the top flange were smaller than 200 MPa when a CFRP load of 66.9 kN (as the maximum load in the acceptance tests) was applied. It is noted that in the proposed clamping system, the application of fillets at the end of the top and bottom plates played an important role in reducing the stress concentration in highly stressed regions.

Performance of the clamping system under fatigue loading

Test set-up

The fatigue performance of the developed clamping system was investigated in the test set-up shown in Fig. 14-a and b. The set-up consisted of two IPB 400 stringers, each with a span of 2.66 m, connected to an IPB 550 floor-beam with a span of 1 m, using four L160×160×15 web-to-web bolted angles. The other ends of the stringers rested on rolling supports. All the parts were made of S235 steel. The vertical cyclic loads were applied on the stringers using two 500-kN Amsler hydraulic actuators located at the mid-span of each stringer. The strengthening system was installed in the set-up as shown in the figure. More detailed information about the

476 dimensions of the set-up is available in Fig. A4 in the appendix. As the clamping system was
477 later used to strengthen the connections in the old riveted bridge in Switzerland, the stringer
478 section and the angle connections used in the set-up had the same dimensions as those of the
479 bridge.

480 The fatigue tests were performed under load-control condition, with a load ratio $R = 0.1$ and
481 a maximum load of 240 kN per actuator. The loading frequency was 4.35 Hz, and the load
482 levels were monitored using two pressure gauges. The prestressing force of each CFRP rod was
483 50 kN (equivalent to 995 MPa) in all the fatigue tests.

484 ***Stress in the CFRP rods***

485 Before application of the fatigue loadings, each CFRP rod (i.e., rods A and B) was pre-
486 stressed up to 50 kN. To apply the desired prestressing force, the strains in each CFRP rod were
487 measured using the strain gauges (type 1-LY66-6/120, HBM AG, Germany) during the pump-
488 ing of the hydraulic cylinders. Fig. 15 shows the stresses in the CFRP rods during the fatigue
489 tests. In total, 11.2 million cycles were applied by the actuators. The measurements from the
490 strain gauges indicate that the stress range in the CFRP rod was approximately 20 MPa. During
491 the fatigue test, no prestressing loss occurred. The fluctuations in the stresses, shown in Fig.
492 15-c, were caused by the daily temperature changes in the laboratory.

493 **Effect of the strengthening system on the stresses in the connections**

494 Prior to the fatigue tests, static tests were also conducted to evaluate the effect of the
495 strengthening system on the connection behavior. In the static tests, the vertical load per actua-
496 tor was increased from 0 to 240 kN (maximum force in the fatigue tests), with different pre-
497 stressing levels, P, in the CFRP rods.

498 ***Description of the FE model developed for the connection tests***

To investigate the stress state in the connections in the test set-up shown in Fig. 14, an FE model was developed, as illustrated in Fig. 16-a; this figure shows the planes of symmetry and the boundary conditions. As the model contained two symmetry planes, only a quarter of the set-up was modeled.

To model the rolling support, on which the floor-beam rested, a reference point RF_3 was defined, with a constraint in the *y*- (vertical) direction. Then, the end section surface of the floor-beam was tied to the reference point. For the rolling support of the stringer, first, the reference point RF_1 was defined, and the corresponding surface was tied to it. Next, RF_1 was connected to the fixed reference point, RF_2, using a nonlinear spring. The function of the nonlinear spring was to constrain the stringer in the vertical direction only when it moved downward (i.e. there would be no constraint on the stringer when an uplift from the support occurred). Therefore, in this model, the stiffness of the spring was extremely high (i.e., sufficient to be considered as infinity) in compression and was zero in tension.

In addition, through the nonlinear spring, it was possible to consider the effect of imperfections. In the set-up shown in Fig. 14, the elevations of the supports were not identical for all supports. In addition, the stringer was not completely straight. Therefore, it was possible that when the stringer was connected to the floor-beam by angles, the other side of the stringer did not perfectly rest on the rolling support. Appendix B provides more information about the manner in which the imperfections were considered in the FE model through the nonlinear spring, as well as the significance of the imperfections.

All parts in the model, i.e., the stringer, floor-beam, and angle, were modeled as isotropic elastic materials with an elastic modulus of 200 GPa and a Poisson's ratio of 0.3. The elements were 3D solid, quadratic reduced-integration type for angle and linear type for stringer and floor-beam.

The mesh sizes of the stringer and the floor-beam were 25 and 15 mm, respectively. For the

524 angle, an optimum value of 3 mm for the mesh size was finalized on the basis of a mesh sensi-
525 tivity study. The contact condition between different parts was similar to that described in the
526 FE model of the beam and the clamping system, i.e., a surface-to-surface discretization with
527 finite sliding formulation, isotropic directionality, “Hard Contact” for normal behavior and the
528 penalty friction formulation for tangential behavior, with a friction coefficient of 0.16.

529 The analysis was performed separately for two different conditions: unstrengthened and
530 strengthened. The steps used for the analysis of the unstrengthened case were as follows:

531 (1) Bolt loads: After the initial step, a bolt force of 100 kN for each bolt (M18, 8.8) was
532 applied as a pressure load around the bolt holes.

533 (2) External load: In the next step, the vertical cylinder load was applied at the mid-span
534 of the stringer, as a pressure load on a surface, as shown in Fig. 16-a, resulting in a
535 120-kN force (only half of the cylinder load applied in the experiment was considered
536 be-cause of the symmetry).

537 For the analysis of the strengthened case, the following steps were used:

538 (1) Bolt loads: These were same as in the first step for the unstrengthened case; however,
539 in this cases, no bolt load was applied around the hole through which the CFRP rod
540 passed.

541 (2) CFRP Load: In this step, the prestressing load P was applied, as shown in Fig. 16-a.

542 (3) Cylinder load: It was same as in the second step for unstrengthened case.

543 In the model, the surface of the stringer top flange, which was below the bottom plate of the
544 clamping system, was tied to the reference point, RF_4, and the prestressing load, P, was applied
545 to this reference point. RF_4 was located in the same position as the CFRP was in the set-up.

546 The FE results show that the critical location was in the angle, where the von Mises and
547 maximum principal stresses were simultaneously maximum, exactly on the angle fillet, as
548 shown in Fig. 16-b. The most stressed part was the back leg of the angle (i.e., the leg of the

549 angle that was connected to the stringer). It is worth mentioning that a change in the arrange-
550 ment of the bolts could alter the stress distribution and the critical location, shifting it to the
551 fillet towards the outstanding leg (i.e., the leg of the angle connected to the floor-beam).

552 ***Experimental results***

553 At the critical location, a multiaxial stress state existed; i.e., not only were the tensile
554 stresses significant, but the shear stresses were also high. Therefore, in the set-up and in the
555 critical locations, instead of normal strain gauges, rosette strain gauges (type 1-RY91-3/120,
556 HBM AG, Germany) were used in the hot spots of the connections. Strain gauges (1) and (2)
557 in Fig. 17-a, were rosette strain gauges, while the other two were normal strain gauges. The
558 strain gauges were placed on the two angles connected to the stringer on the left side, with a
559 layout similar to that shown in Fig. 17-b. No strain gauge was placed on the other two connec-
560 tions on the stringer on the right side.

561 The strains measured using the strain gauges were used to verify the FE model. The meas-
562 ured strains in the *a*-, *b*-, and *c*- directions were compared with the FE results for both the
563 unstrengthened and strengthened cases.

564 In this paper, the results of only the measurements using rosette strain gauge (1) are pre-
565 sented, as depicted in Fig. 18. As shown in this figure, the FE model was capable of accurately
566 predicting the strains in different directions. In addition, the results show that the strains in the
567 *a*-direction were negligible, while the strains in the *c*-direction were the highest. The reason
568 was that the out-of-plane deformation of the angles mainly applied tensile strains (or stresses)
569 in the *c*-direction due to local bending in the angle connections.

570 Furthermore, the results show the effectiveness of the strengthening system in reducing the
571 strains, especially in the *c*-direction. The application of 50 kN of prestressing to the CFRP rods
572 reduced the strains in the *c*-direction from 813 to 468 microstrain (i.e., approximately 42%
573 reduction), and from 555 to 354 microstrain in the *b*-direction. The reduction of the strains, and

574 consequently the stresses, in the critical location of the connections was the result of the reduc-
575 tion in the out-of-plane deformation of the angles.

576 Using the verified FE model, for a cylinder load of 120 kN, the different components of the
577 stress tensor at the critical node before and after strengthening (50 kN per rod) are summarized
578 in Table 3. With this information, it was possible to distinguish the dominant stress components,
579 and evaluate the effect of strengthening system on each stress component.

580 As given in Table 3, the strengthening system reduced the stress components significantly.
581 The stress reduction for the components σ_z and τ_{xz}, which had the highest values among all,
582 was 42% each. Therefore, it could be inferred that the proposed strengthening system was ca-
583 pable of effectively increasing the fatigue life of the connections. In addition, the results in
584 Table 3 reveal the importance of considering the multiaxial state of stress in the critical location.

585 Notably, the determination of appropriate multiaxial fatigue criteria for the prevention of fa-
586 tigue cracks in the critical locations of the angles, in which the strengthening effect was also
587 incorporated, is crucial. Discussing the multiaxial theoretical models together with experi-
588 mental verifications is beyond the scope of this study and will be taken up as a follow-up study
589 by the authors in the future.

590 **Field application of the proposed strengthening system**

591 After a demonstration of the reliable and effective performance of the strengthening system
592 in a laboratory, the proposed clamping system was applied on the Aabach Bridge, which is an
593 old riveted railway bridge in Lachen, Switzerland, as shown in Fig. 19.

594 The prestressing level in each of the CFRP rods (on both sides of the stringers) was 50 kN,
595 which was 994.7 MPa and 49% of the CFRP nominal ultimate tensile strength. For long-term
596 monitoring of the prestressing level in the CFRP rods, a wireless sensor network (WSN) system

597 was applied on the bridge, as shown in the figure. Therefore, for at least one year, any prestress-
598 ing loss in the CFRP rods due to the slippage of the clamping system or of the rods inside the
599 barrels would be monitored. In addition, for protection against corrosion and galvanic corrosion
600 between different materials inside the wedge-barrel system, a plastic cap was used on the
601 wedge-barrel anchors, as shown in the figure. A comprehensive coverage of the field applica-
602 tion is beyond the scope of this study and will be performed in a subsequent study.

603 **Summary and conclusions**

604 This paper presents a retrofit solution that can be used for strengthening bridge connections
605 with minimal damage and interventions (i.e., without closing the bridge or enforcing any traffic
606 management). The strengthening system reduces the out-of-plane deformation and stresses in
607 the angle connections using prestressed CFRP rods. The retrofit system consists of a newly
608 developed wedge-barrel anchor and a friction-based clamping system. Prestressed CFRP rods
609 are used (rather than strips) as they can easily pass through the connection (in the openings
610 made by removing bolts/rivets). A simple presetting system was also developed, enabling the
611 application of high presetting forces on-site for the installation of the wedge-barrel system. The
612 installation procedure requires a few temporary plates and housing, and includes assembling,
613 presetting, and prestressing (of the CFRP rods using a hydraulic jack). Furthermore, it is possi-
614 ble to disassemble the system using the same temporary parts without any residual effect on the
615 original structure. The clamping system consists of different plates, which are bolted together
616 and grab the flange of the steel beam. The prestressing force of the CFRP rod is transmitted to
617 the beam solely through friction, without the need for drilling holes and without damaging the
618 parent steel structure. The key findings of this study are summarized as follows:

619 ***Results of the static pull-off tests***

620 • The slippage load of the system was 128 kN, which was greater than 100% of the actual
621 CFRP ultimate tensile strength of 2367 MPa (i.e., 119 kN).

- No slippage occurred between the components during pulling of the CFRP rods, either in the clamping system or in the wedge-barrel anchors.
- When the CFRP load exceeded a certain level, both the wedges and the CFRP rod moved simultaneously further into the barrel, which was the desired behavior for the anchors.
- A detailed FE model was developed to simulate the retrofit system and optimize its dimen-sions and performance. The stresses in different parts of the clamping system, as well as in the top flange of the clamped stringer, were observed to remain below the yield stress of the material in all the parts.

Results of the fatigue tests

- A novel set-up for testing bridge connections was designed and used in this study. The test set-up included four supports, which could simulate the complexities of the boundary con-ditions of bridge connections.
- A series of fatigue tests was performed on the steel connections with dimensions identical to those in a riveted railway bridge in Switzerland. The proposed strengthening system was demonstrated to be capable of reducing the stresses at critical locations (hotspots) in the angle connections by more than 40%.
- The fatigue results showed that the designed retrofit system could survive more than 11 million load cycles, without any damage to the CFRP rods, connections, and clamping system. Furthermore, there was no indication of any loss in the CFRP prestress level during cyclic loading.
- Using a detailed FE model, the effects of geometrical imperfections during the installation of different components of the connections were extensively discussed and verified by laboratory measurements. The steel connections were also modeled before and after strengthening, and the results of the FE model correlated well with experimental measurements obtained in the laboratory.

- After the successful design and completion of the laboratory static and fatigue tests, the maintenance system was finally used for strengthening the old steel bridge. The long-term performance of the system is currently being monitored using a wireless monitoring system.

Recommendations for future studies

- The proposed strengthening system can be further optimized for different applications. Development of a strengthening system consisting of a clamping system and an anchor head with multiple prestressed CFRP rods (rather than a single rod) for applications in which a high prestressing force is required would be recommended.
- In addition, to identify the appropriate multiaxial fatigue criteria for predicting the fatigue failure in the stringer-to-floor-beam angle connections, experimental and numerical investigations have to be conducted.

Data Availability Statement

Some or all data, models, or code that support the findings of this study are available from the corresponding author upon reasonable request.

Acknowledgements

This work has been funded primarily by the Innosuisse Swiss Innovation Agency (Grant ID: 12993.1 PFIW-IW). The authors would also like to acknowledge the financial and technical support from S&P Clever Reinforcement Company AG, Switzerland; the Swiss Federal Railways (SBB) AG, Bern; and dsp Ingenieure + Planer AG Engineering Office, Uster, Switzerland, for this project. They also thank the technicians from the Structural Engineering Research Laboratory of Empa for their outstanding collaborations during the experiments. Finally, the scientific and technical support from Dr. Ardalan Hosseini, postdoctoral scholar at the University of California, Davis, in different stages of the design of the strengthening system is highly appreciated.

672 **Appendix**

673 **A. Detailed dimensions of the clamping system and different set-ups**

674 The detailed dimensions of the parts used in the clamping system, housing, static pull-off
675 test, and set-up for the fatigue tests on the connections are shown in Figs. A1, A2, A3, and A4,
676 respectively.

677 **B. FE modeling of the imperfections in the connection tests**

678 As mentioned in the section regarding the FE model developed for the connection tests, due
679 to the presence of imperfections in the set-up shown in Fig. 14, there can be a gap distance Δ
680 between the stringer and the rolling support, as shown in Fig. B1-a. In this case, stresses are
681 formed in the connection when the stringer touches the support, because of the stringer self-
682 weight during the installation process. In the laboratory tests, when the values of the strain
683 gauges were reset to zero.

684 When a prestressing force is applied in the CFRP rod, an uplift occurs in the support due to
685 the sagging bending moment (see Fig. B1-b). At this stage, the strain gauges display compres-
686 sive strains in the top of the connections. Due to the application of the external (cylinder) loads,
687 the stringer rests on the support, as demonstrated in Fig. B1-c.

688 The effect of Δ in the FE model was simulated with a nonlinear spring. To model the non-
689 linear spring in ABAQUS, as shown in Fig. B2, the stiffness of the spring in tension was taken
690 as zero because there was no constraint on the stringer for upward deflection on the support in
691 the set-up. When the spring was compressed up to $-\Delta$, no force was generated in the spring
692 (i.e., the stiffness was zero). When the compressive deformation in the spring was greater than
693 $-\Delta$, the stiffness of the spring would become extremely high (i.e., high enough to be considered
694 to be infinity). The $\delta - F$ relationship considered in ABAQUS is given in Fig. B2.

695 The effect of Δ on the strain in the c-direction of the strain gauge (1) (see Fig. 17-a) is
696 depicted graphically in Fig. B3. When the external load was low, the stringer actually behaved

similar to a cantilever beam (see Fig. B1-c). Therefore, the strain in the connection increased rapidly. When the stringer touched the support, the rate of increase of the strain in the connections decreased because of the change in the static condition (boundary condition) of the stringer.

As shown in Fig. B3, for low load levels (< 50 kN), when the effect of Δ was not considered (i.e., $\Delta = 0$), the experimental and the FE results differed significantly. However, taking $\Delta = 0.8$ mm provided a good agreement between the FE model and experimental results. In this study, $\Delta = 0.8$ mm was considered for the FE model. As evident, when the external load level was high (> 50 kN), this effect was negligible because the stringer had already rested on the support.

References

Al-Emrani, M. 2002. "Fatigue in Riveted Railway Bridges-a study of the fatigue performance of riveted stringers and stringer-to-floor-beam connections". *Chalmers University of Technology*.

Al-Emrani, M., and R. Kliger. 2009. "Fatigue prone details in steel bridges". *Nordic Steel Construction Conference*.

Al-Mayah, A., K. Soudki, and A. Plumtree. 2005. "Gripping Behavior of CFRP PrestressingRods for Novel Anchor Design." *Special Publication.* 230: 209-228.

Al-Mayah, A., K. Soudki, and A. Plumtree. 2006a. "Development and assessment of a new CFRP rod–anchor system for prestressed concrete." *Applied Composite Materials.* 13(5): 321-334.

Al-Mayah, A., K. Soudki, and A. Plumtree. 2006b. "FEM and mathematical models of the interfacial contact behaviour of CFRP-metal couples." *Composite Structures.* 73(1): 33-40.

Al-Mayah, A., K. Soudki, and A. Plumtree. 2007. "Novel anchor system for CFRP rod: Finite-element and mathematical models." *Journal of Composites for Construction.* 11(5): 469-476.

722 Baker, K., and G. Kulak. 1985. "Fatigue of riveted connections." *Canadian Journal of Civil*
723 *Engineering.* 12(1): 184-191.
724 Bennitz, A., J. W. Schmidt, J. Nilimaa, B. Täljsten, P. Goltermann, and D. L. Ravn. 2012.
725 "Reinforced concrete T-beams externally prestressed with unbonded carbon fiber-reinforced
726 polymer tendons." *ACI Structural Journal.* 109(4): 521.
727 Bowman, M. D. 2012. "Fatigue evaluation of steel bridges". *Transportation Research Board*.
728 Campbell, T., N. G. Shrive, K. Soudki, A. Al-Mayah, J. Keatley, and M. Reda. 2000. "Design
729 and evaluation of a wedge-type anchor for fibre reinforced polymer tendons." *Canadian*
730 *Journal of Civil Engineering.* 27(5): 985-992.
731 Dassault Systèmes. 2014. ABAQUS 6.14 analysis user's manual, Dassault Systems Inc
732 Waltham, USA.
733 Dawood, M., S. Rizkalla, and E. Sumner. 2007. "Fatigue and overloading behavior of steel-
734 concrete composite flexural members strengthened with high modulus CFRP materials."
735 *Journal of Composites for Construction.* 11(6): 659-669.
736 EOTA. 2002. ETAG 013 Guideline for European Technical Approval of Post-Tensioning Kits
737 for Prestressing of Structures, EOTA Brussels, Belgium.
738 Fisher, J. W., B. Yen, D. Wang, and J. Mann. 1987. "Fatigue and fracture evaluation for rating
739 riveted bridges".
740 Fisher, J. W., B. T. Yen, and D. Wang. 1990. "Fatigue strength of riveted bridge members."
741 *Journal of structural Engineering.* 116(11): 2968-2981.
742 Fritsch, E., M. Izadi, and E. Ghafoori. 2019. "Development of nail-anchor strengthening system
743 with iron-based shape memory alloy (Fe-SMA) strips." *Construction and Building Materials.*
744 229: 117042.DOI: https://doi.org/10.1016/j.conbuildmat.2019.117042.
745 Ghafoori, E. 2015. Fatigue strengthening of metallic members using un-bonded and bonded
746 CFRP laminates, ETH Zurich.

747 Ghafoori, E. 2019. "Editorial for special issue on Sustainable Metallic Structures." *Engineering*
748 *Structures.* 183: 83.DOI: https://doi.org/10.1016/j.engstruct.2018.12.086.
749 Ghafoori, E., A. Hosseini, R. Al-Mahaidi, X.-L. Zhao, and M. Motavalli. 2018. "Prestressed
750 CFRP-strengthening and long-term wireless monitoring of an old roadway metallic bridge."
751 *Engineering Structures.* 176: 585-605.DOI: https://doi.org/10.1016/j.engstruct.2018.09.042.
752 Ghafoori, E., and M. Motavalli. 2015a. "Innovative CFRP-Prestressing System for
753 Strengthening Metallic Structures." *Journal of Composites for Construction.* 19(6):
754 04015006.DOI: 10.1061/(ASCE)CC.1943-5614.0000559.
755 Ghafoori, E., and M. Motavalli. 2015b. "Lateral-torsional buckling of steel I-beams retrofitted
756 by bonded and un-bonded CFRP laminates with different pre-stress levels: experimental and
757 numerical study." *Construction and Building Materials.* 76: 194–206.DOI: doi:
758 10.1016/j.conbuildmat.2014.11.070.
759 Ghafoori, E., M. Motavalli, J. Botsis, A. Herwig, and M. Galli. 2012. "Fatigue strengthening of
760 damaged metallic beams using prestressed unbonded and bonded CFRP plates." *International*
761 *Journal of Fatigue.* 44: 303-315.
762 Ghafoori, E., M. Motavalli, A. Nussbaumer, A. Herwig, G. Prinz, and M. Fontana. 2015a.
763 "Design criterion for fatigue strengthening of riveted beams in a 120-year-old railway metallic
764 bridge using pre-stressed CFRP plates." *Composites Part B: Engineering.* 68: 1-13.
765 Ghafoori, E., M. Motavalli, A. Nussbaumer, A. Herwig, G. Prinz, and M. Fontana. 2015b.
766 "Determination of minimum CFRP pre-stress levels for fatigue crack prevention in retrofitted
767 metallic beams." *Engineering Structures.* 84: 29–41.DOI: doi:10.1016/j.engstruct.2014.11.017.
768 Haghani, R. 2014. "Analysis of adhesive joints between fibre-reinforced polymer laminates and
769 structural steel members." *Australian Journal of Structural Engineering.* 15(4): 393-406.
770 Haghani, R., M. Al-Emrani, and M. Heshmati. 2012. "Fatigue-prone details in steel bridges."
771 *Buildings.* 2(4): 456-476.

772 Haghani, R., M. Al-Emrani, and R. Kliger. 2009. "Interfacial stress analysis of geometrically
773 modified adhesive joints in steel beams strengthened with FRP laminates." *Construction and*
774 *Building Materials.* 23(3): 1413-1422.
775 osseini, A., E. Ghafoori, R. Al-Mahaidi, X.-L. Zhao, and M. Motavalli. 2019a. "Strengthening
776 of a 19th-century roadway metallic bridge using nonprestressed bonded and prestressed
777 unbonded CFRP plates." *Construction and Building Materials.* 209: 240-259.DOI:
778 https://doi.org/10.1016/j.conbuildmat.2019.03.095.
779 Hosseini, A., E. Ghafoori, M. Motavalli, A. Nussbaumer, X.-L. Zhao, and R. Al-Mahaidi.
780 2018a. "Flat prestressed unbonded retrofit system for strengthening of existing metallic I-
781 Girders." *Composites Part B: Engineering.* 155: 156-172.
782 Hosseini, A., E. Ghafoori, M. Motavalli, A. Nussbaumer, X.-L. Zhao, R. Al-Mahaidi, and G.
783 Terrasi. 2019b. "Development of prestressed unbonded and bonded CFRP strengthening
784 solutions for tensile metallic members." *Engineering Structures.* 181: 550-561.DOI:
785 https://doi.org/10.1016/j.engstruct.2018.12.020.
786 Hosseini, A., E. Ghafoori, M. Motavalli, A. Nussbaumer, X.-L. Zhao, and R. Koller. 2018b.
787 "Prestressed Unbonded Reinforcement System with Multiple CFRP Plates for Fatigue
788 Strengthening of Steel Members." *Polymers.* 10(3): 264.
789 Hosseini, A., E. Ghafoori, M. Motavalli, A. Nussbaumer, X. L. Zhao, and R. Al-Mahaidi.
790 2018c. "Flat Prestressed Unbonded Retrofit System for Strengthening of Existing Metallic I-
791 Girders." *Composites Part B.* 155: 156-172.
792 Hosseini, A., J. Michels, M. Izadi, and E. Ghafoori. 2019c. "A comparative study between Fe-
793 SMA and CFRP reinforcements for prestressed strengthening of metallic structures."
794 *Construction and Building Materials.* 226: 976-992.DOI:
795 https://doi.org/10.1016/j.conbuildmat.2019.07.169.

796 Izadi, M., A. Hosseini, J. Michels, M. Motavalli, and E. Ghafoori. 2019a. "Thermally activated
797 iron-based shape memory alloy for strengthening metallic girders." *Thin-Walled Structures.*
798 141: 389-401.DOI: https://doi.org/10.1016/j.tws.2019.04.036.
799 Izadi, M., M. Motavalli, and E. Ghafoori. 2019b. "Iron-based shape memory alloy (Fe-SMA)
800 for fatigue strengthening of cracked steel bridge connections." *Construction and Building*
801 *Materials.* 227: 116800.DOI: https://doi.org/10.1016/j.conbuildmat.2019.116800.
802 Izadi, M. R., E. Ghafoori, M. Motavalli, and S. Maalek. 2018a. "Iron-based shape memory alloy
803 for the fatigue strengthening of cracked steel plates: Effects of re-activations and loading
804 frequencies." *Engineering Structures.* 176: 953-967.DOI:
805 https://doi.org/10.1016/j.engstruct.2018.09.021.
806 Izadi, M. R., E. Ghafoori, M. Shahverdi, M. Motavalli, and S. Maalek. 2018b. "Development
807 of an iron-based shape memory alloy (Fe-SMA) strengthening system for steel plates."
808 *Engineering Structures.* 174: 433-446.
809 Kianmofrad, F., E. Ghafoori, M. M. Elyasi, M. Motavalli, and M. Rahimian. 2017.
810 "Strengthening of metallic beams with different types of pre-stressed un-bonded retrofit
811 systems." *Composite Structures.* 159: 81-95.DOI:
812 http://dx.doi.org/10.1016/j.compstruct.2016.09.020.
813 Kuehn, B., M. Lukic, A. Nussbaumer, H.-P. Günther, R. Helmerich, S. Herion, M. H. Kolstein,
814 S. Walbridge, B. Androic, and O. Dijkstra. 2008. Assessment of existing steel structures:
815 recommendations for estimation of remaining fatigue life, Joint Research Center.
816 Kulak, G. L., J. W. Fisher, and J. H. Struik. 2001. "Guide to Design Criteria for Bolted and
817 Riveted Joints Second Edition."
818 Meier, U. 1995. "Extending the life of cables by the use of carbon fibers". *Proc., International*
819 *Association for Bridge and Structural Engineering Symp*.

820 Mertz, D. R., and J. W. J. Gillespie. 1996. "Rehabilitation of steel bridge girders through the
821 application of advanced composite materials." *Contract NCHRP-93-ID011. Transportation*
822 *Research Board, Washington, D.C.*
823 Munse, W., and K. Petersen. 1959. "Strength of rivets and bolts in tension." *Journal of the*
824 *Structural Division.* 85(3): 7-28.
825 Recommendation, F. 1993. "Recommendations for the acceptance of post-tensioning systems."
826 *1993.*
827 Reemsnyder, H. S. 1975. "Fatigue life extension of riveted connections." *Journal of the*
828 *Structural Division.* 101(ASCE# 11795 Procceding)
829 Roeder, C. W., G. MacRae, A. Leland, and A. Rospo. 2005. "Extending the fatigue life of
830 riveted coped stringer connections." *Journal of Bridge Engineering.* 10(1): 69-76.
831 Rostásy, F. S. 1998. "Draft guidelines for the acceptance testing of FRP posttensioning
832 tendons." *Journal of Composites for Construction.* 2(1): 2-6.
833 Sayed-Ahmed, E. Y., and N. G. Shrive. 1998. "A new steel anchorage system for post-
834 tensioning applications using carbon fibre reinforced plastic tendons." *Canadian Journal of*
835 *Civil Engineering.* 25(1): 113-127.
836 Schmidt, J. W., A. Bennitz, B. Täljsten, P. Goltermann, and H. Pedersen. 2012. "Mechanical
837 anchorage of FRP tendons–A literature review." *Construction and Building Materials.* 32: 110-
838 121.
839 Schmidt, J. W., A. Bennitz, B. Täljsten, and H. Pedersen. 2010. "Development of mechanical
840 anchor for CFRP tendons using integrated sleeve." *Journal of Composites for Construction.*
841 14(4): 397-405.
842 Schmidt, J. W., S. T. Smith, B. Täljsten, A. Bennitz, P. Goltermann, and H. Pedersen. 2011.
843 "Numerical simulation and experimental validation of an integrated sleeve-wedge anchorage
844 for CFRP rods." *Journal of Composites for Construction.* 15(3): 284-292.

845 Schnerch, D., M. Dawood, S. Rizkalla, and E. Sumner. 2007. "Proposed design guidelines for
846 strengthening of steel bridges with FRP materials." *Construction and Building Materials.* 21(5):
847 1001-1010.
848 Wriggers, P., and G. Zavarise. 2004. "Computational contact mechanics." *Encyclopedia of*
849 *computational mechanics.*
850 Zhao, X.-L. 2013. "FRP-strengthened metallic structures". *CRC Press*.

Table 1

Table 1. Summary of the results of the static pull-off tests

Test no.	Ultimate CFRP force (kN)	Maximum CFRP stress (MPa)	Failure mode
1	104	2070	CFRP rupture
2	109	2168	CFRP rupture
3	112	2228	CFRP rupture
4	114	2268	CFRP rupture

Table 2

Table 2. Mesh sizes in different parts in the FE model

Case	Mesh size (mm)							
	Hallow shaft	Spacer	Stiffeners	Top plate	Bottom plate	Vertical plate	Beam	
							Fine mesh region	Coarse mesh region
Fine mesh	5	3	5	5	5	5	5	30
Coarse mesh	5	3	5	10	10	10	8	30

Table 3

Table 3. Strengthening effect on different stress components

Stage	Stress level (MPa)					
	σ_x	σ_y	σ_z	τ_{xy}	τ_{xz}	τ_{yz}
Before Strengthening	33.6	44	146.4	11.3	–65.1	–24
After Strengthening	18.9	26.4	84.5	8.4	-37.7	–18.3
Reduction (%)	44	40	42	26	42	24

Figure 1

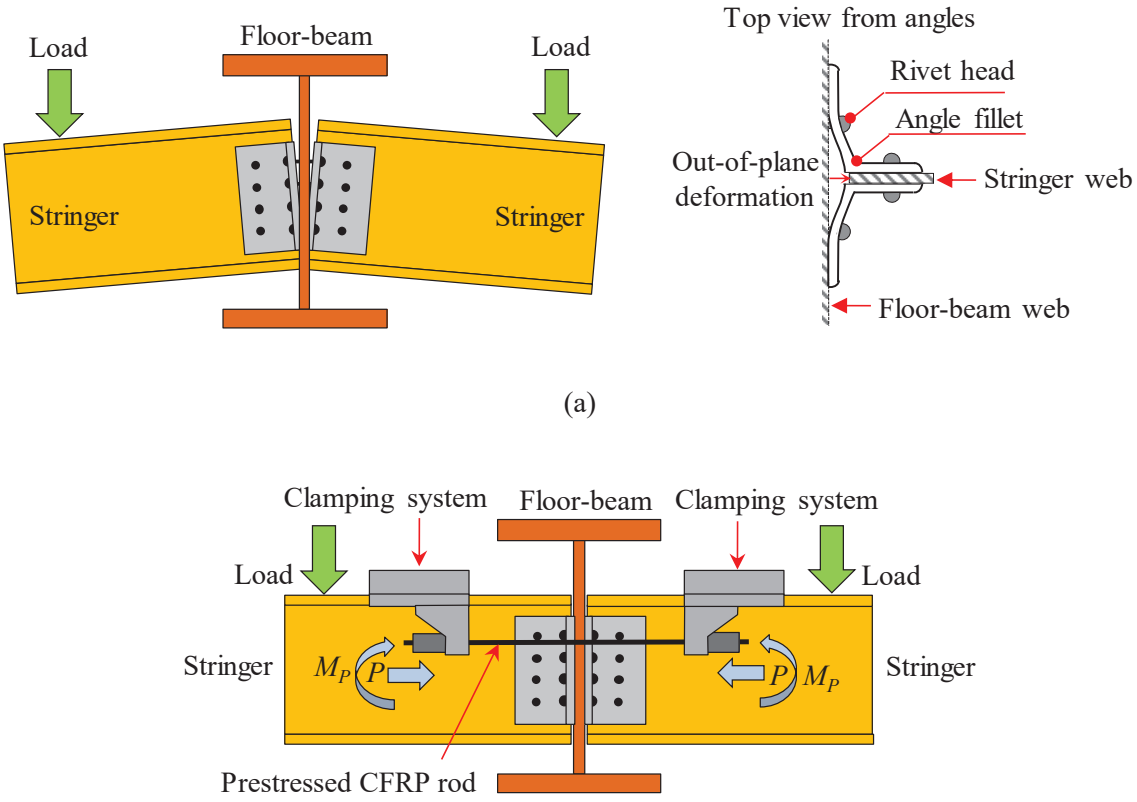

Fig. 1. Out-of-plane deformation in stringer-to-floor-beam connections: (a) Out-of-plane deformation due to superimposed load on the stringers and the potential failure locations in the connections; (b) Concept of the proposed strengthening system to reduce out-of-plane deformation.

Figure 2

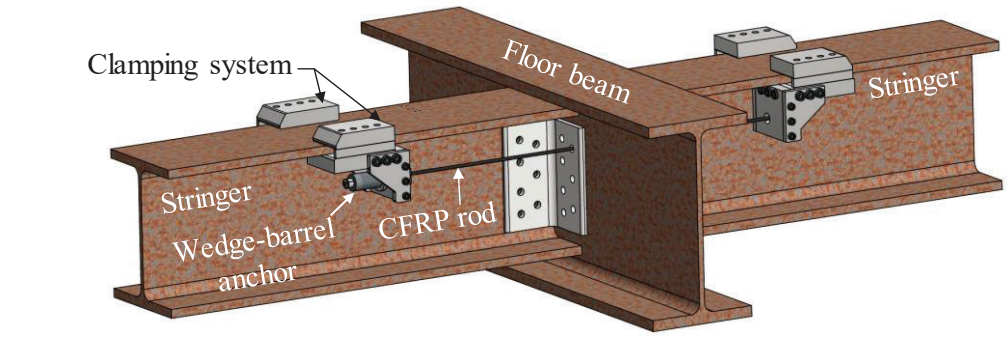

(a)

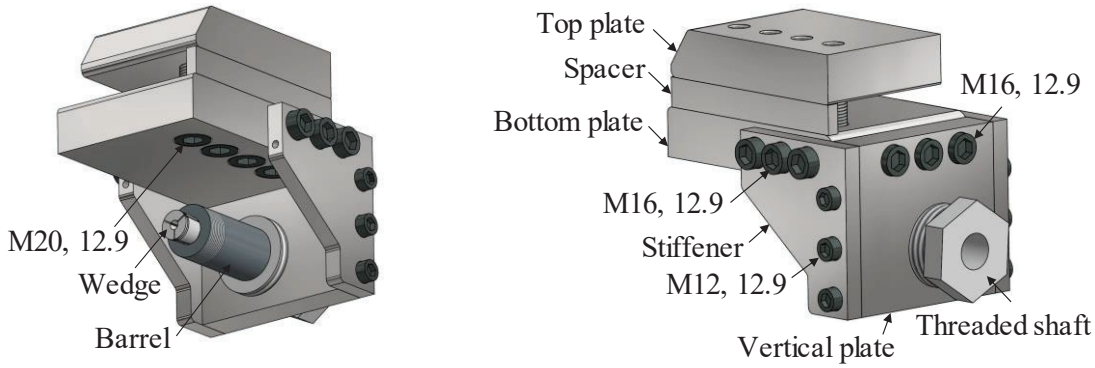

(b)

Fig. 2. Proposed strengthening system for double-angle stringer-to-floor-beam connections: (a) Configuration of the proposed strengthening system; (b) Different parts of the strengthening system.

Figure 3

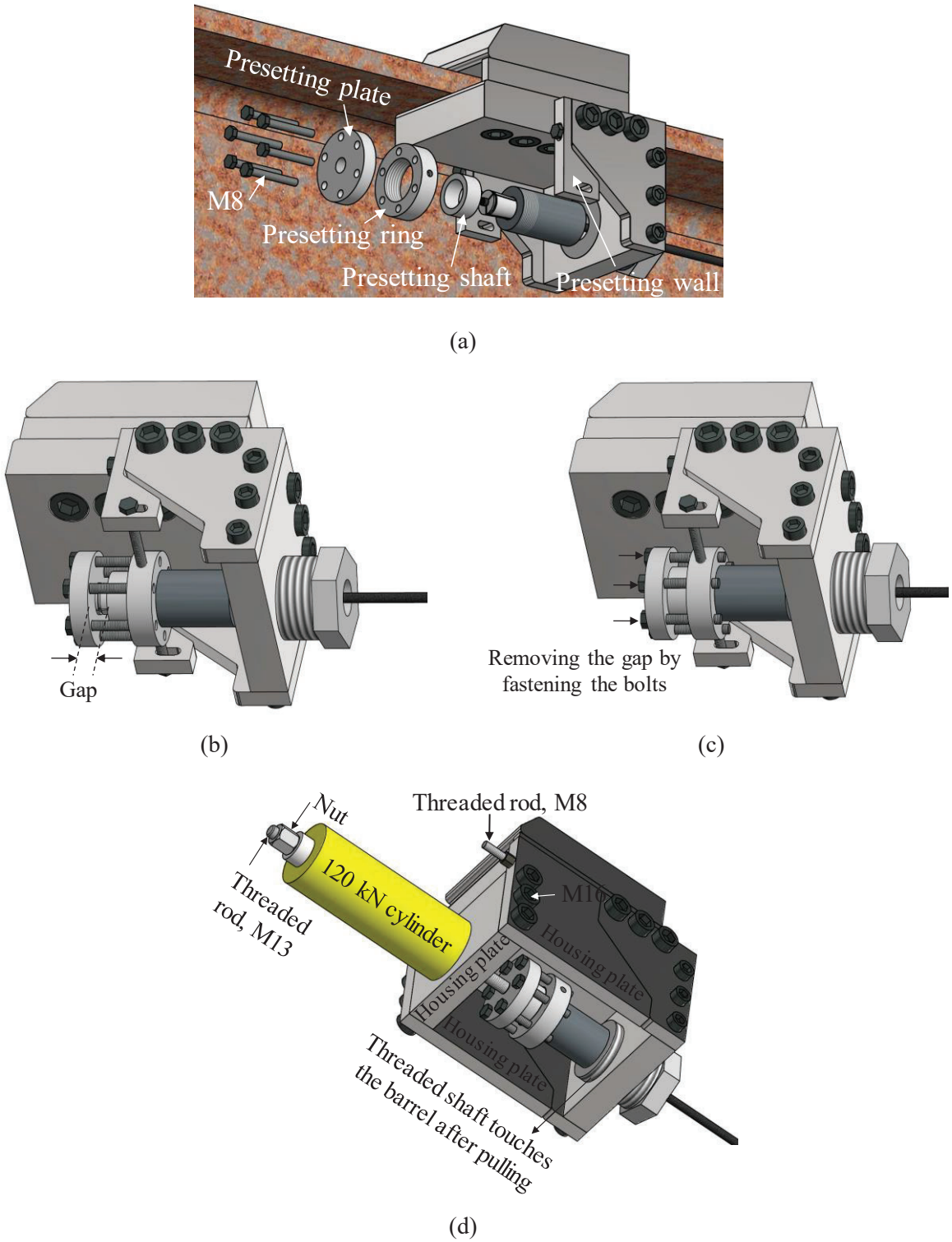

Fig. 3. Presetting and prestressing procedures: (a) Required parts for presetting; (b) Before fastening the presetting bolts; (c) After fastening the presetting bolts; (d) Prestressing procedure.

Figure 4

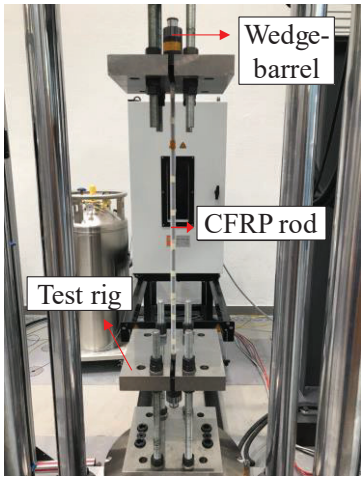

(a)

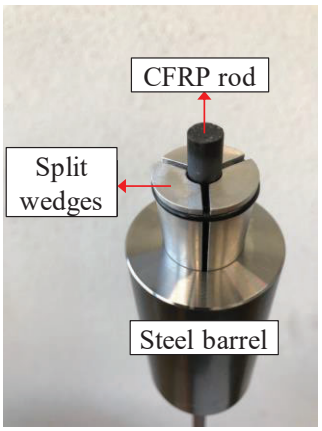

(b)

Fig. 4. Wedge-barrel anchor developed at Empa: (a) The test set-up for uniaxial static and fatigue tests; (b) Components of the wedge-barrel anchor.

Figure 5

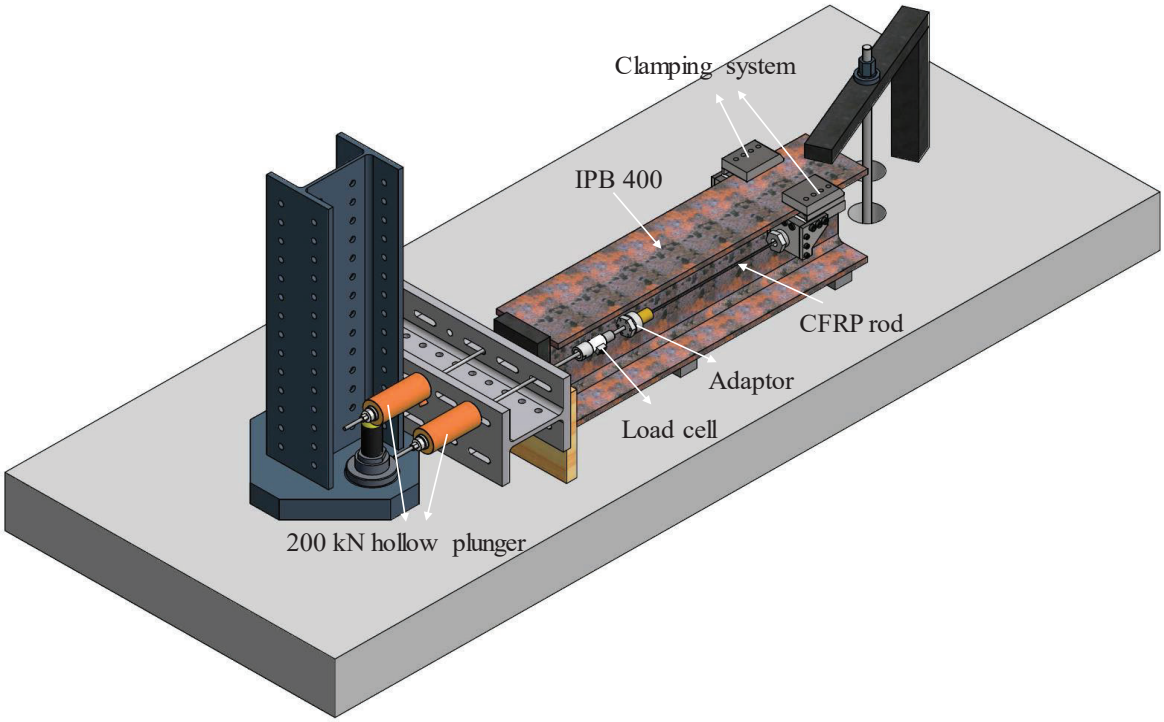

Fig. 5. Test set-up for the static pull-off tests.

Figure 6

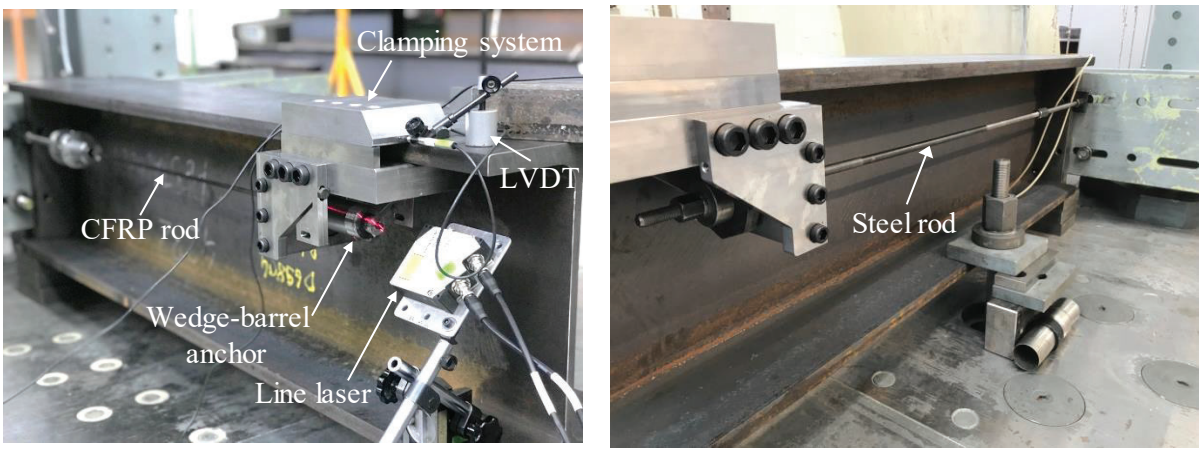

(a) (b)

Fig. 6. Details of the clamping system on each side of the beam: (a) Clamping system on the left side; (b) Clamping system on the right side.

Figure 7

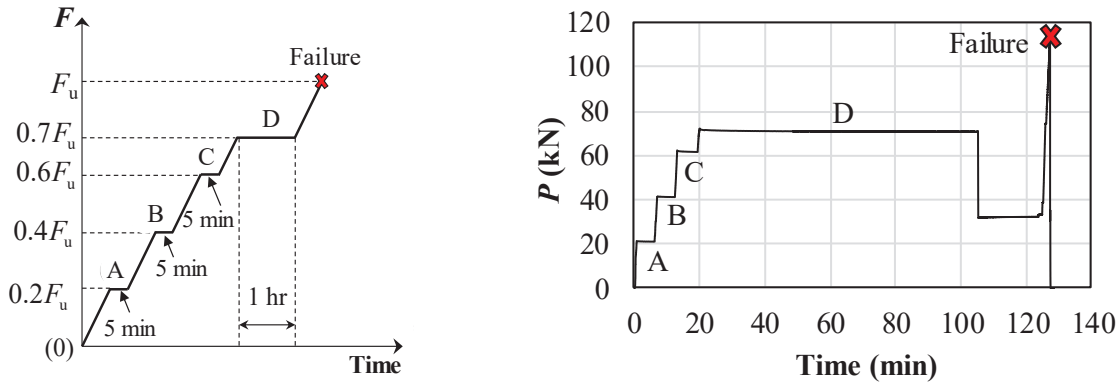

(a) (b)

Fig. 7. Loading protocol in the static pull-off tests: (a) Protocol proposed in (Rostásy 1998); (b) Applied load in the pull-off tests.

Figure 8

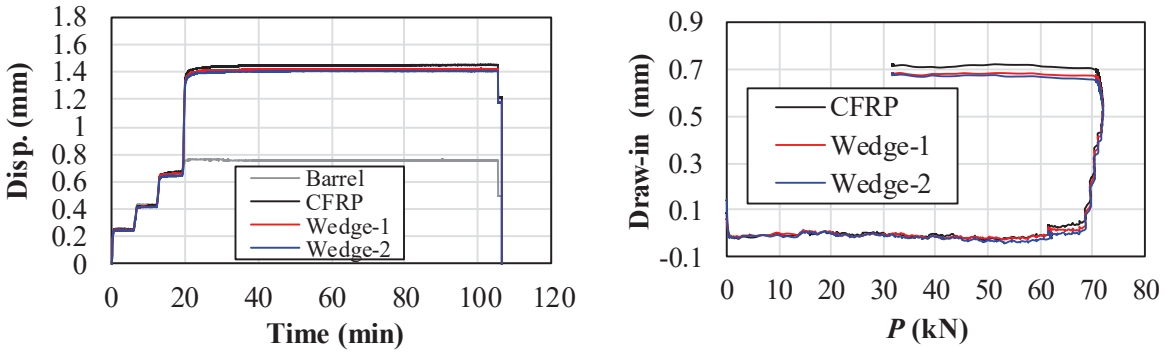

(a) (b)

Fig. 8. Measurements in the wedge-barrel anchor during the static pull-off tests: (a) Displacement of the wedge-barrel components; (b) Draw-ins.

Figure 9

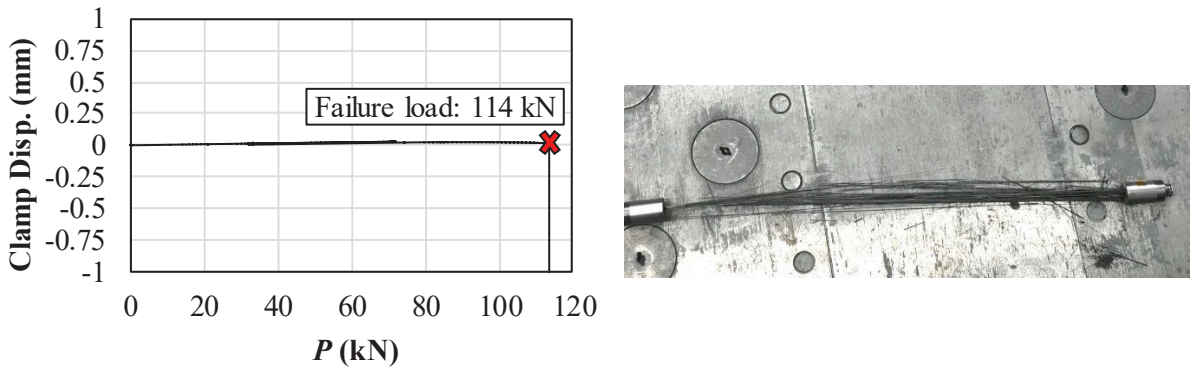

(a) (b)

Fig. 9. The experimental results from test no. 4: (a) Load-displacement curve of the clamp; (b) Failed CFRP rod.

Figure 10

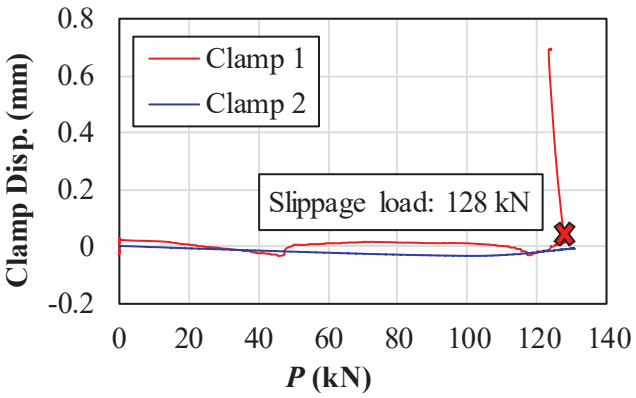

Fig. 10. Slippage load of the clamping system.

Figure 11

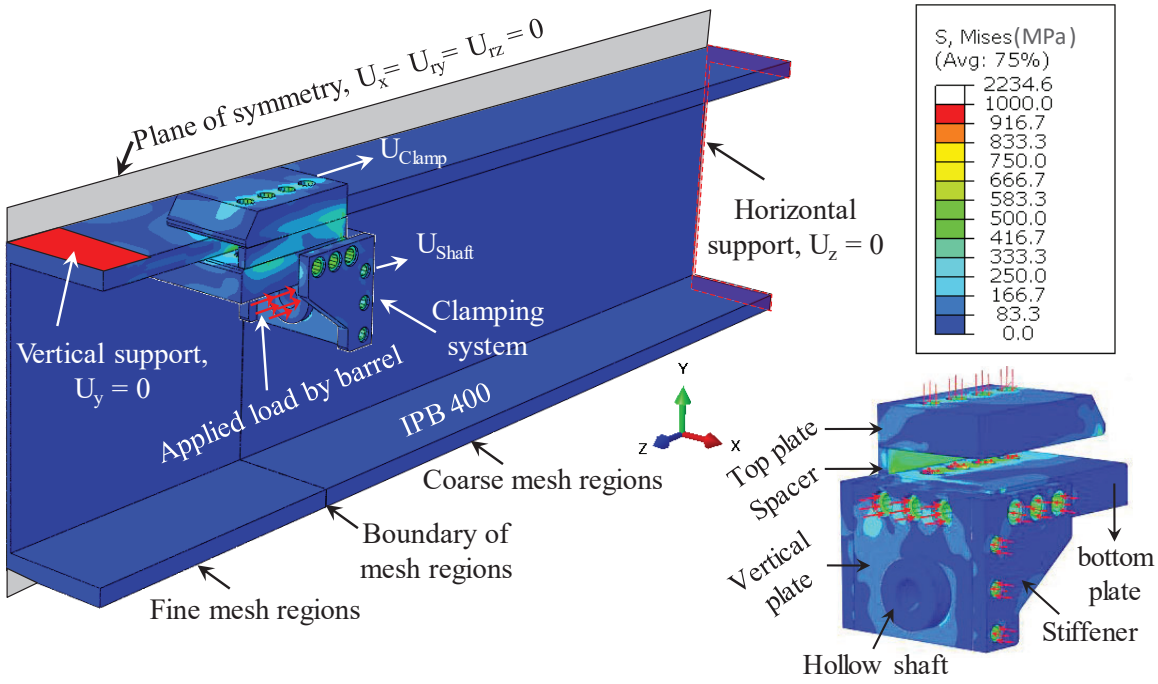

Fig. 11. FE model of the beam and the clamping system, with the von Mises stress distribution under a load of 125 kN (slippage load).

Figure 12

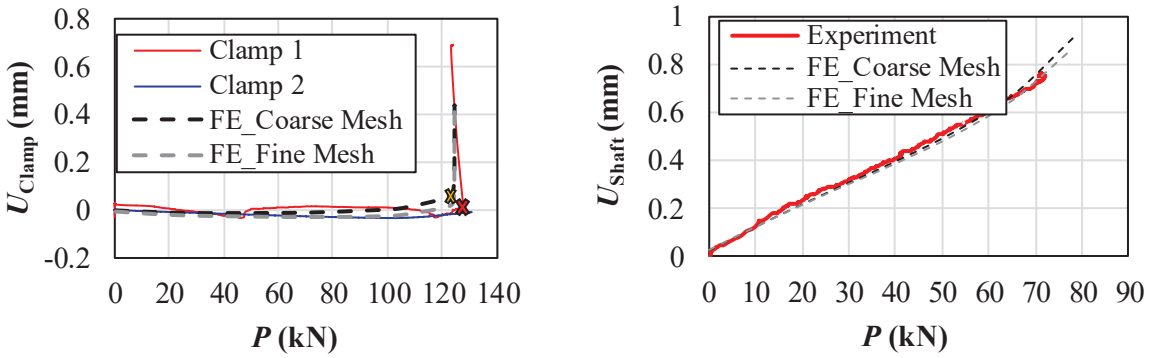

(a) (b)

Fig. 12. Verification of the FE model with the experimental results: (a) Slippage load of the whole clamping system; (b) Displacement of the threaded hollow shaft in the loading direction.

Figure 13

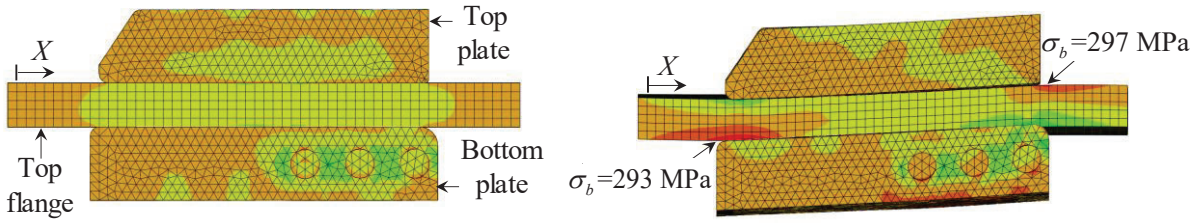

(a) (b)

Fig. 13. Tensile stresses in the top flange due to the rotation of the clamp: (a) Undeformed shape (P = 0); (b) Deformed shape (P = 125 kN).

Figure 14

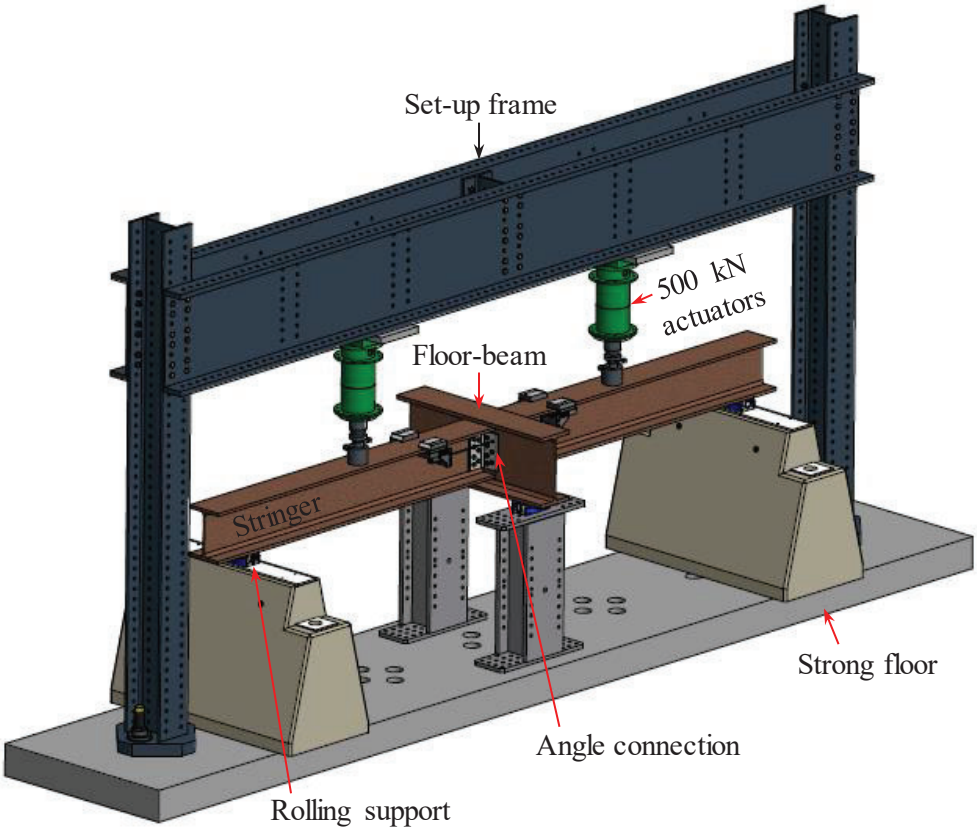

(a)

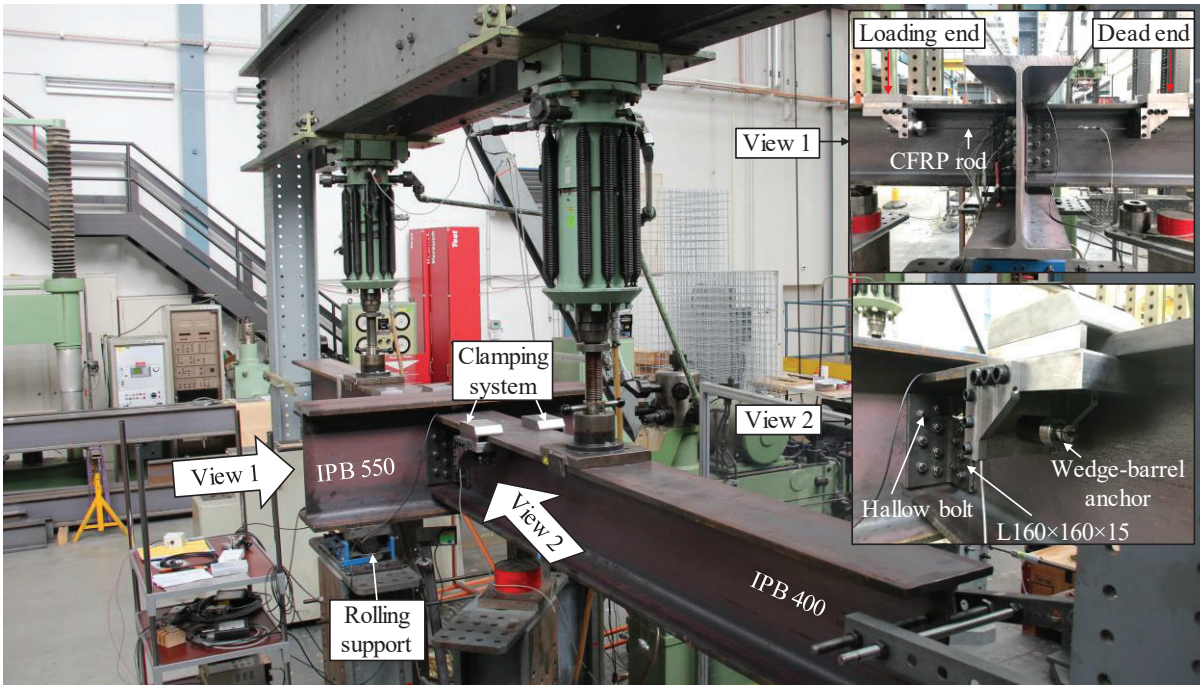

(b)

Fig. 14. Test set-up for the fatigue tests: (a) Overview of the fatigue test set-up; (b) Details of the fatigue test set-up.

Figure 15

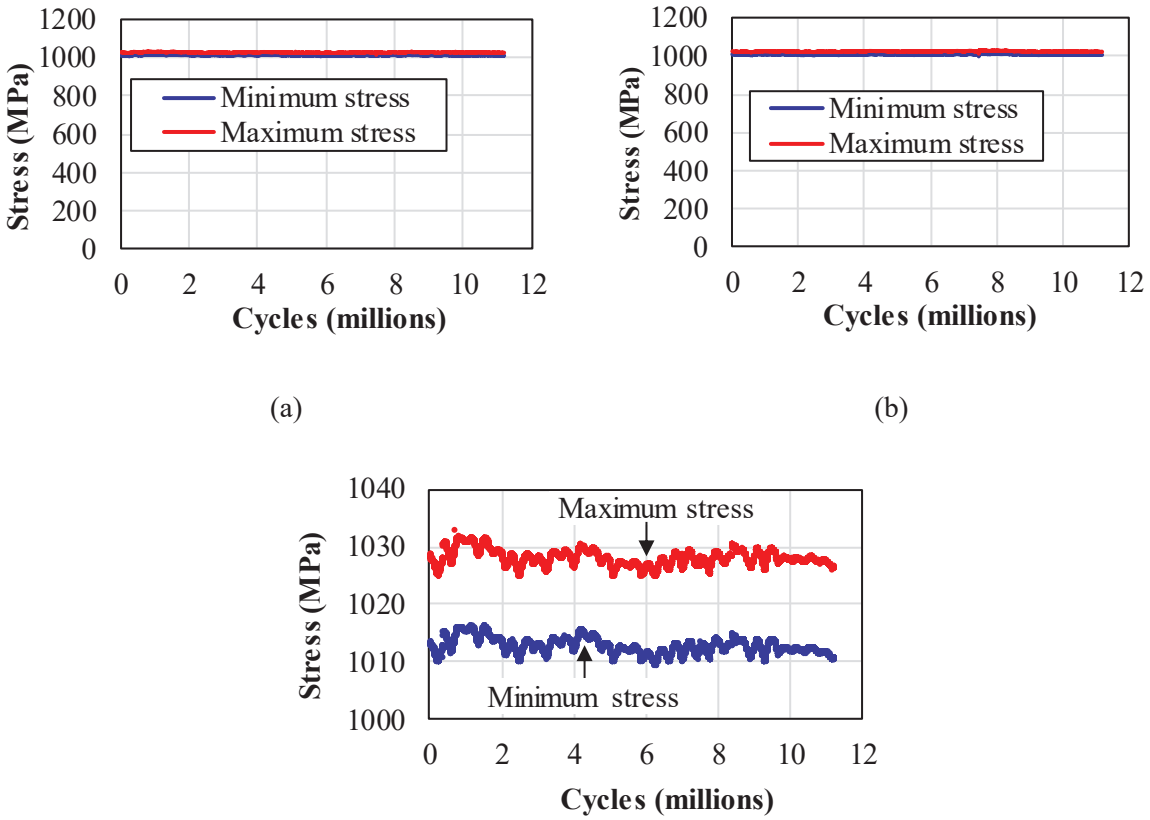

Fig. 15. Stress in the CFRP rods during the fatigue loading: (a) Stress in CFRP_A; (b) Stress in CFRP_B; (c) Daily variation of cyclic stresses in CFRP_A.

Figure 16

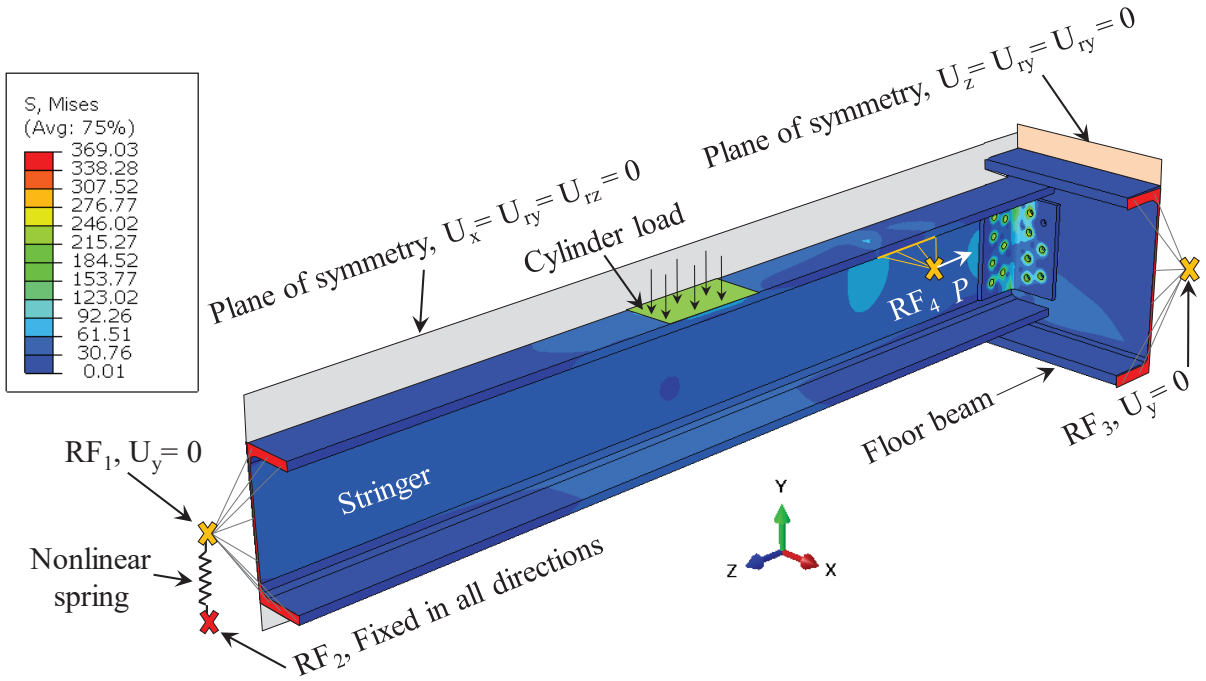

(a)

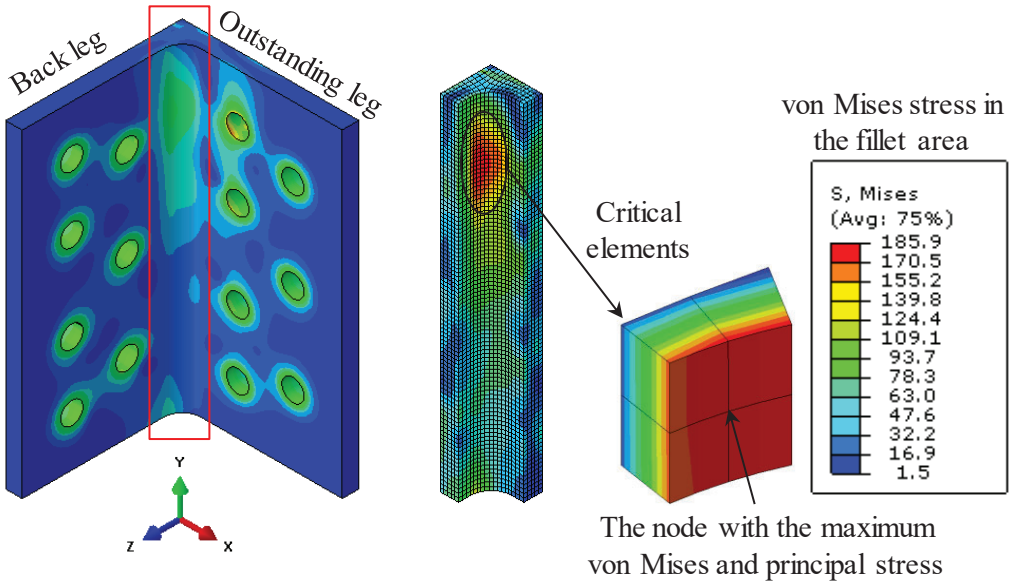

(b)

Fig. 16. FE model of the connection tests set-up: (a) Details of the ¼ FE model and the von Mises stress distribution under a cylinder load of 120 kN (in model); (b) Critical location in the angle.

Figure 17

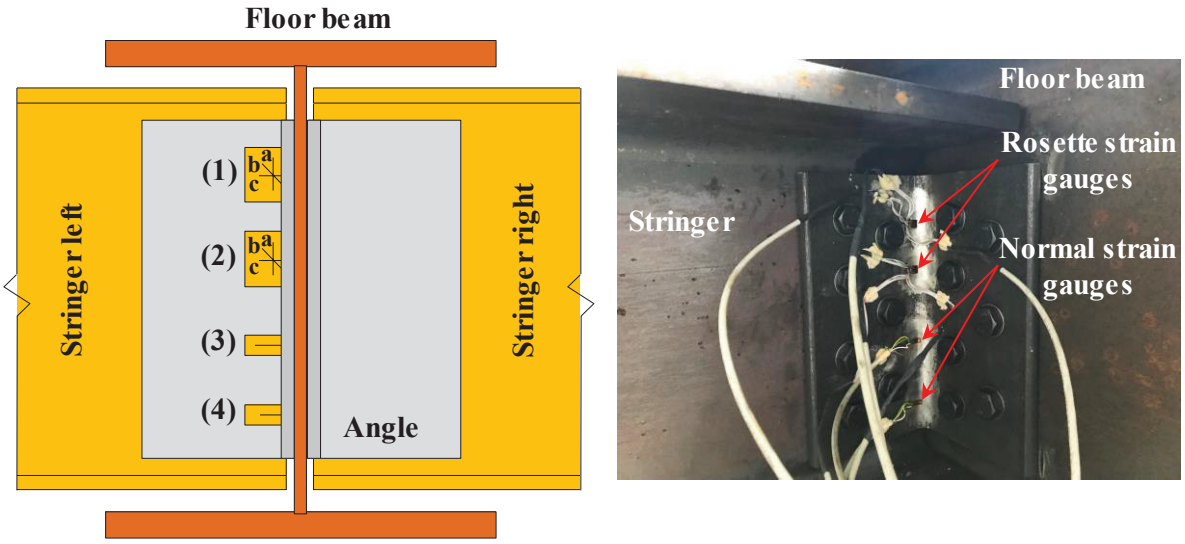

(a) (b)

Fig. 17. Strain gauges used for the measurement of strain state in the connections: (a) Schematic of the arrangement of rosette and normal strain gauges; (b) Strain gauges applied on the connection.

Figure 18

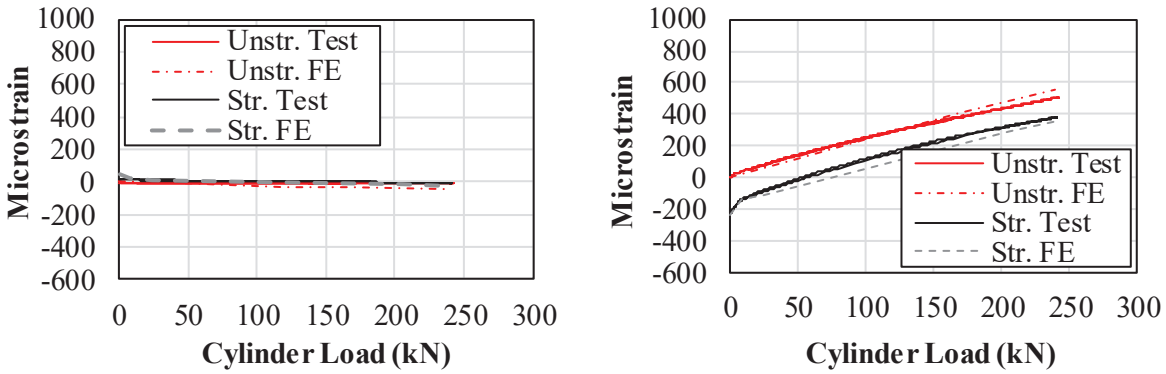

(a) *a*-direction

(b) *b*-direction

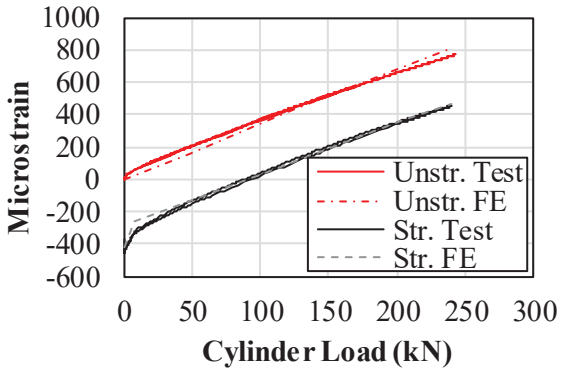

(c) *c*-direction

Fig. 18. Strain components in the angles based on the measurements from strain gauge (1): (a) *a*-direction; (b) *b*-direction; (c) *c*-direction.

Figure 19

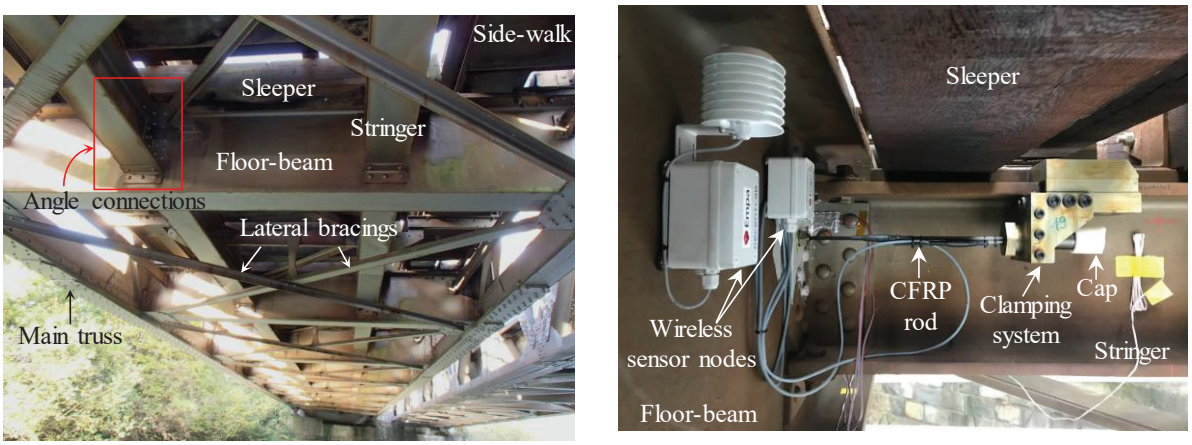

(a) (b)

Fig. 19. Application of the proposed strengthening system on Aabach Bridge, Lachen, Switzerland: (a) Different elements of the bridge floor system; (b) Installed system on the bridge.

Figure A1

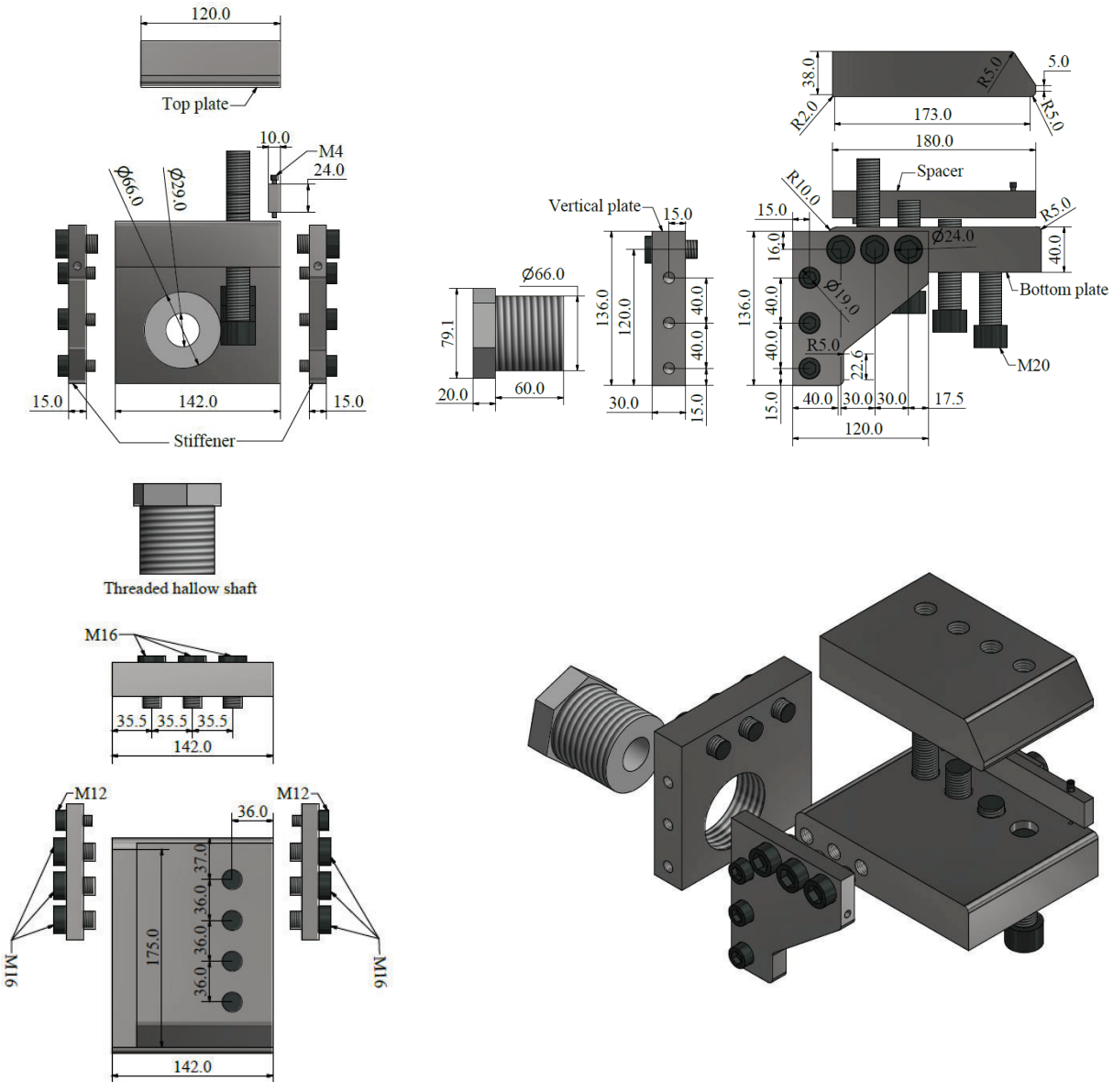

Fig. A1. Details and dimensions of different components of the clamping system.

Figure A2

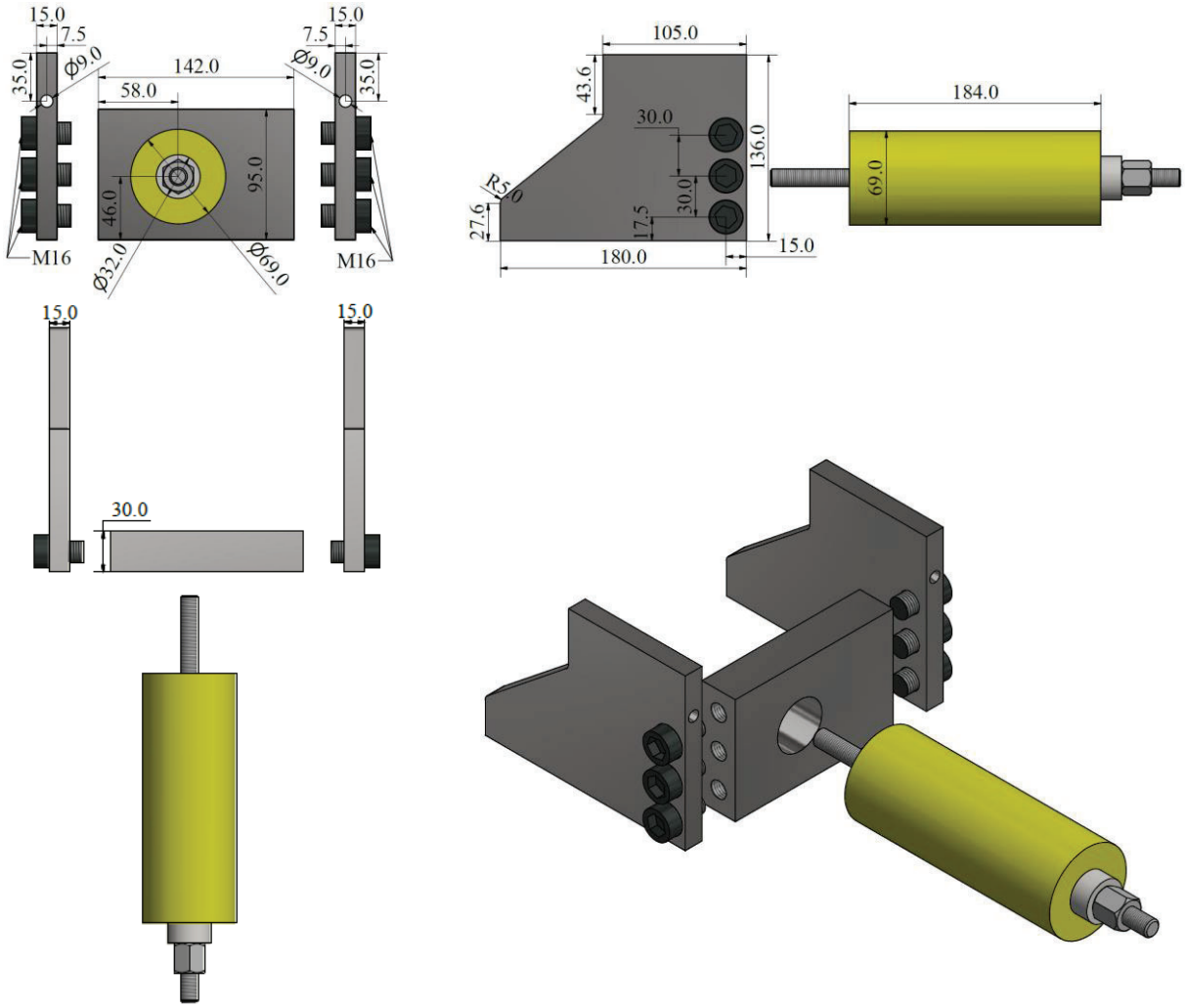

Fig. A2. Details and dimensions of the housing system.

Figure A3

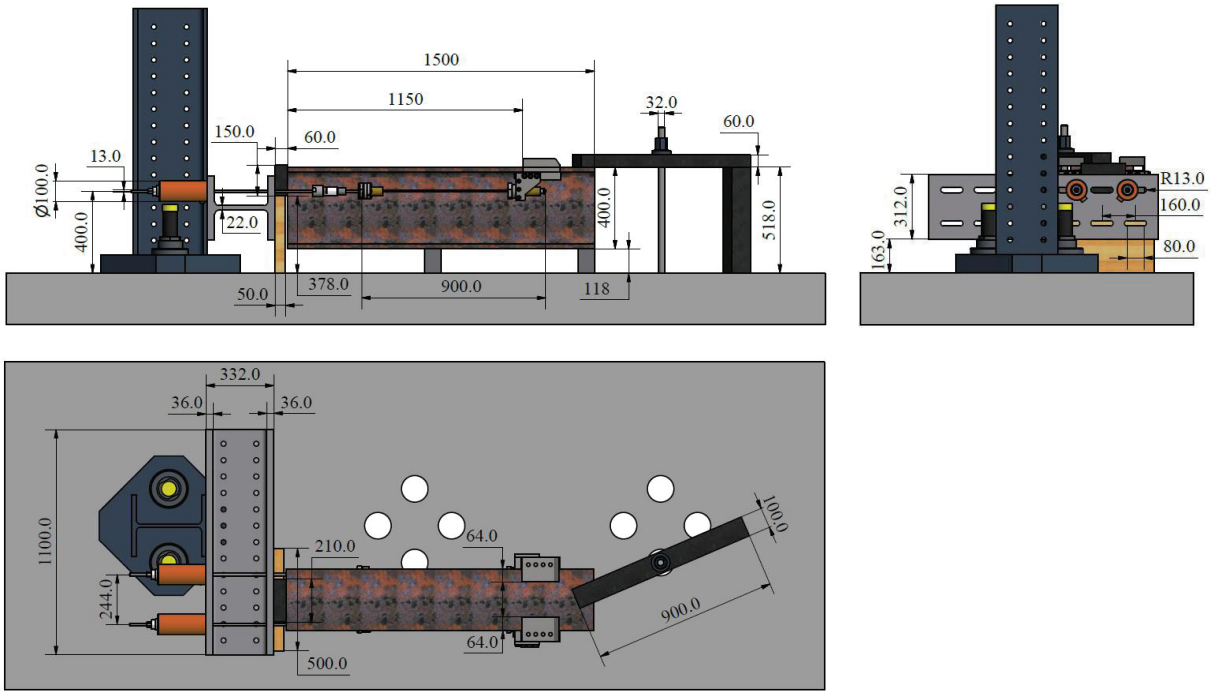

Fig. A3. Details and dimensions of the components of the static pull-off test.

Figure A4

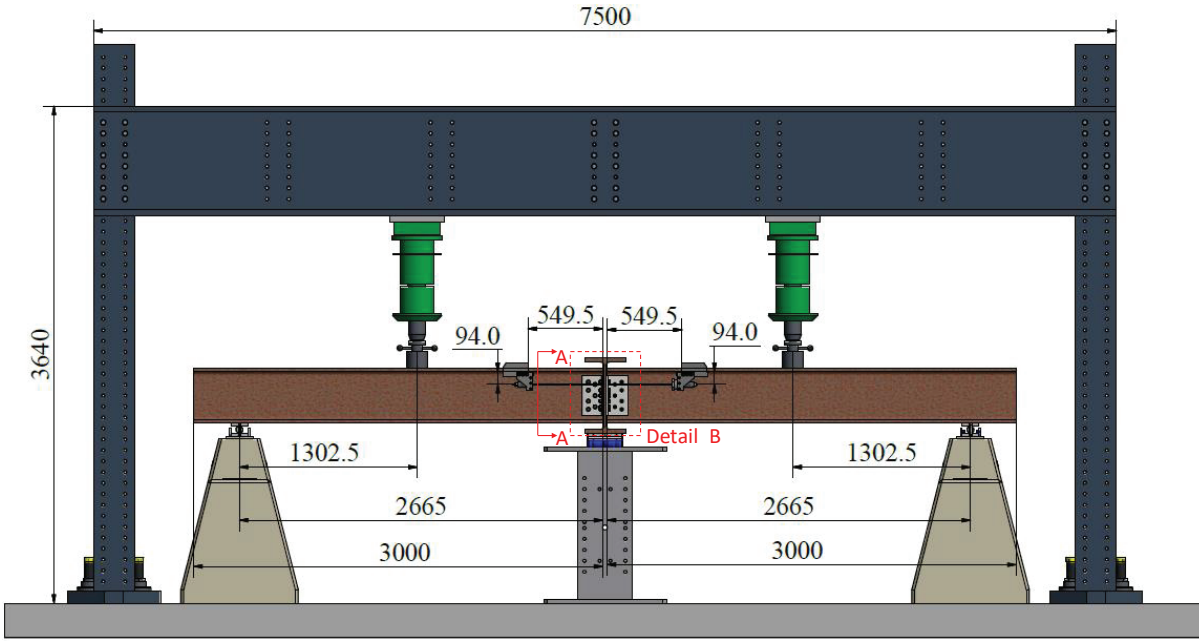

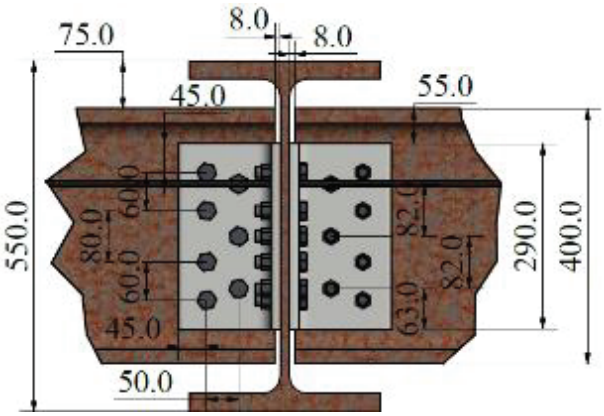

Detail B

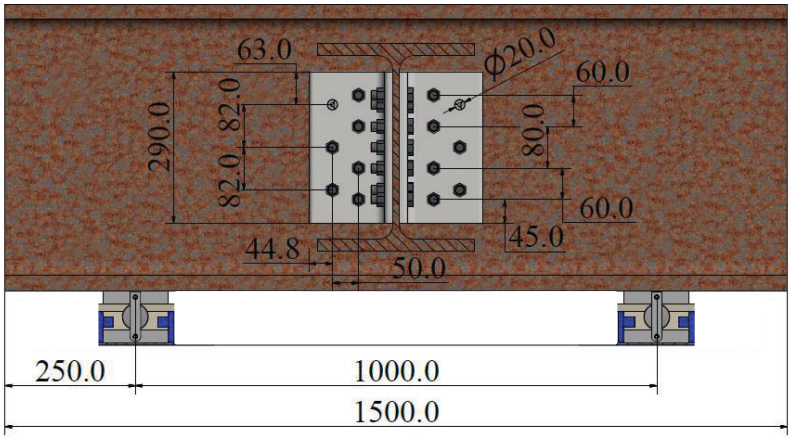

Section A

Fig. A4. Details and dimensions of different components of the set-up for the fatigue tests.

Figure B1

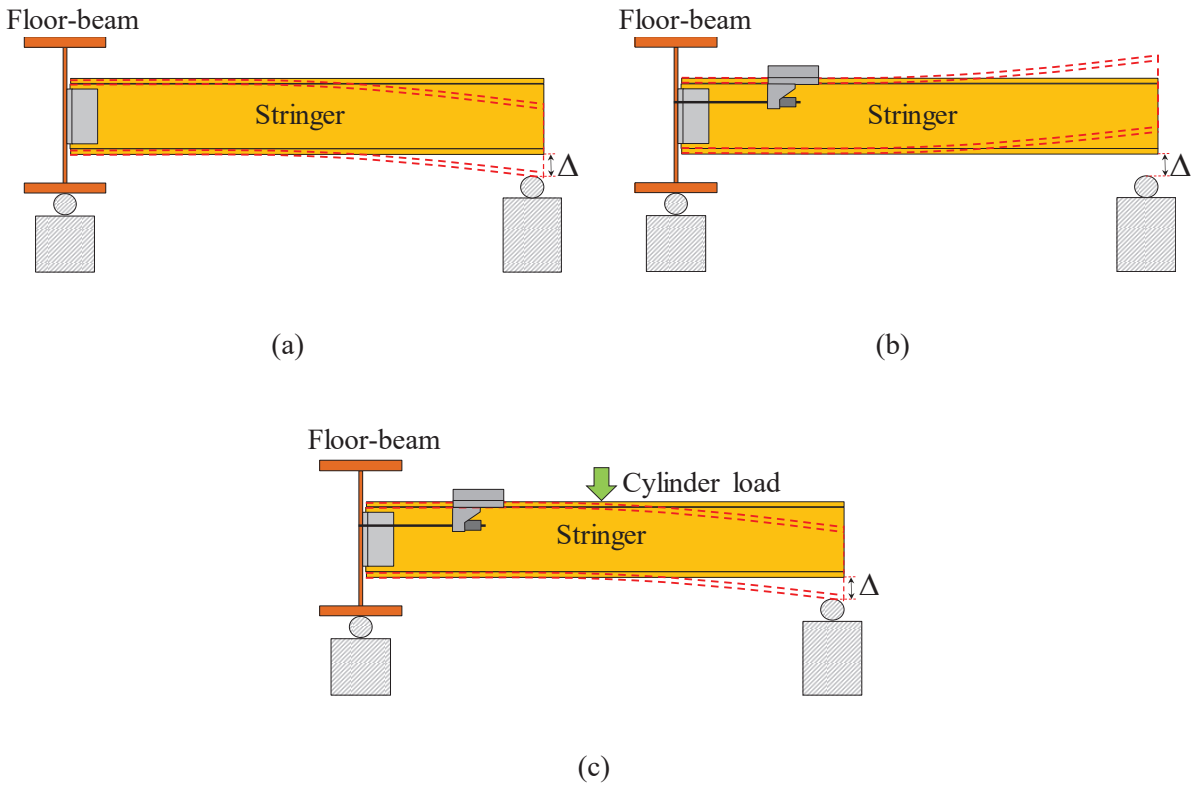

Fig. B1. Deflection of the stringer considering the imperfections: (a) Deflection due to self-weight of the stringer; (b) Deflection due to the prestressing force; (c) Deflection after the application of the cylinder load.

Figure B2

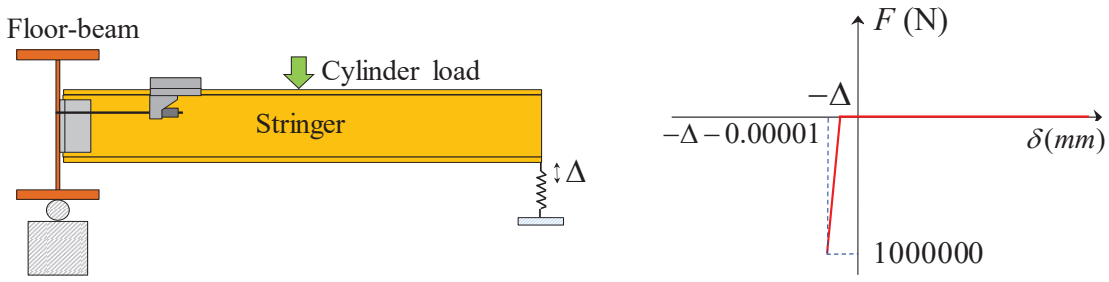

Fig. B2. Modeling the imperfection effect in FE simulation using a nonlinear spring.

Figure B3

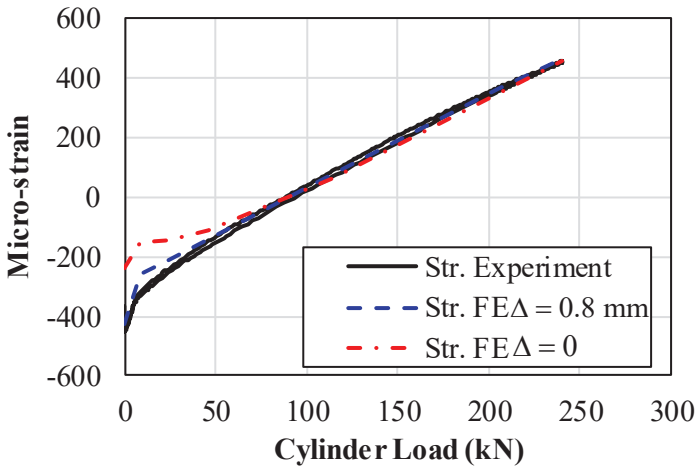

Fig. B3. Effect of gap distance Δ on the strain in the *c*-direction of the strain gauge (1).

Figure caption list:

Fig. 1. Out-of-plane deformation in stringer-to-floor-beam connections: (a) Out-of-plane deformation due to superimposed load on the stringers and the potential failure locations in the connections; (b) Concept of the proposed strengthening system to reduce out-of-plane deformation.

Fig. 2. Proposed strengthening system for double-angle stringer-to-floor-beam connections: (a) Configuration of the proposed strengthening system; (b) Different parts of the strengthening system.

Fig. 3. Presetting and prestressing procedures: (a) Required parts for presetting; (b) Before fastening the presetting bolts; (c) After fastening the presetting bolts; (d) Prestressing procedure.

Fig. 4. Wedge-barrel anchor developed at Empa: (a) The test set-up for uniaxial static and fatigue tests; (b) Components of the wedge-barrel anchor.

Fig. 5. Test set-up for the static pull-off tests.

Fig. 6. Details of the clamping system on each side of the beam: (a) Clamping system on the left side; (b) Clamping system on the right side.

Fig. 7. Loading protocol in the static pull-off tests: (a) Protocol proposed in (Rostásy 1998); (b) Applied load in the pull-off tests.

Fig. 8. Measurements in the wedge-barrel anchor during the static pull-off tests: (a) Displacement of the wedge-barrel components; (b) Draw-ins.

Fig. 9. The experimental results from test no. 4: (a) Load-displacement curve of the clamp; (b) Failed CFRP rod.

Fig. 10. Slippage load of the clamping system.

Fig. 11. FE model of the beam and the clamping system, with the von Mises stress distribution under a load of 125 kN (slippage load).

Fig. 12. Verification of the FE model with the experimental results: (a) Slippage load of the whole clamping system; (b) Displacement of the threaded hollow shaft in the loading direction.

Fig. 13. Tensile stresses in the top flange due to the rotation of the clamp: (a) Undeformed shape ($P = 0$); (b) Deformed shape ($P = 125$ kN).

Fig. 14. Test set-up for the fatigue tests: (a) Overview of the fatigue test set-up; (b) Details of the fatigue test set-up.

Fig. 15. Stress in the CFRP rods during the fatigue loading: (a) Stress in CFRP_A; (b) Stress in CFRP_B; (c) Daily variation of cyclic stresses in CFRP_A.

Fig. 16. FE model of the connection tests set-up: (a) Details of the ¼ FE model and the von Mises stress distribution under a cylinder load of 120 kN (in model); (b) Critical location in the angle.

Fig. 17. Strain gauges used for the measurement of strain state in the connections: (a) Schematic of the arrangement of rosette and normal strain gauges; (b) Strain gauges applied on the connection.

Fig. 18. Strain components in the angles based on the measurements from strain gauge (1): (a) *a*-direction; (b) *b*-direction; (c) *c*-direction.

Fig. 19. Application of the proposed strengthening system on Aabach Bridge, Lachen, Switzerland: (a) Different elements of the bridge floor system; (b) Installed system on the bridge.

Fig. A1. Details and dimensions of different components of the clamping system.

Fig. A2. Details and dimensions of the housing system.

Fig. A3. Details and dimensions of the components of the static pull-off test.

Fig. A4. Details and dimensions of different components of the set-up for the fatigue tests.

Fig. B1. Deflection of the stringer considering the imperfections: (a) Deflection due to self-weight of the stringer; (b) Deflection due to the prestressing force; (c) Deflection after the application of the cylinder load.

Fig. B2. Modeling the imperfection effect in FE simulation using a nonlinear spring.

Fig. B3. Effect of gap distance Δ on the strain in the *c*-direction of the strain gauge (1).